Atmospheric Pollution Research 17 (2026) 103096

Contents lists available at ScienceDirect

Atmospheric Pollution Research

journal homepage: www.elsevier.com/locate/apr

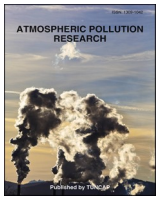

Development and implementation of SOMA: A secondary organic module for aerosol integration in high-resolution air quality simulations

Giannis Ioannidis [a], Nikoletta Bouloti [a], Paul Tremper [b], Chaofan Li [b], Christos Boikos [a], Nikolaos Rapkos [a], Till Riedel [b], Miikka Dal Maso [c], Leonidas Ntziachristos [a,*]

[a] Mechanical Engineering Department, Aristotle University of Thessaloniki, Thessaloniki, GR, 54124, Greece
[b] Karlsruhe Institute of Technology (KIT), TECO/Pervasive Computing Systems, Karlsruhe, 76131, Germany
[c] Aerosol Physics Laboratory, Physics Unit, Faculty of Engineering and Natural Sciences, Tampere University, Tampere, Finland

ARTICLE INFO

Keywords:
SOA
CFD
Air quality
Traffic emissions
SOMA

ABSTRACT

Secondary Organic Aerosols (SOAs) are formed following oxidation of Volatile Organic Compounds (VOCs) in the atmosphere and have a significant contribution to fine particulate matter concentrations. Understanding SOA formation is crucial, particularly in urban environments, where various emission sources contribute across different time scales. To decipher SOA formation dynamics, this study introduces SOMA (Secondary Organic Module for Aerosol) embedded in air quality modelling. SOMA considers VOC oxidation with OH using species concentrations, exposure duration, Nitrogen Oxides (NO_x) levels and SOA yields as inputs, the latter obtained from the GECKO-A model. A total of 113 experiments are gathered from literature, involving four different VOC species (α-pinene, isoprene, limonene, and toluene), to produce correction factors depending on ozone (O_3) levels, relative humidity (RH), and temperature (T). SOMA was linked to CFD modelling and was used to characterise the dispersion of toluene SOA emissions from traffic in a heavily trafficked area in Augsburg, Germany. The dispersion model was used to simulate pollutant recirculation in the examined area using a novel approach by combining both local road traffic emissions and background sources. SOA formation from toluene was examined over a 12-h period. The results indicated that background SOA constituted 21-53% of the identified SOA mass. After 7 h, the influence of background SOA on modelled concentrations became negligible due to precursor consumption and dilution. The combination of high-resolution pollution maps generated by CFD and atmospheric chemistry involving SOA formation enhances the air quality modelling capabilities and can provide valuable information to the scientific community.

1. Introduction

Secondary organic aerosols (SOAs) are formed through the oxidation of Volatile Organic Compounds (VOCs) by atmospheric oxidants such as Hydroxyl Radical (OH), ozone (O_3), and nitrate ion (NO_3), producing low-volatility compounds that partition into the particle phase (Hallquist et al., 2009; Srivastava et al., 2022). OH, formed under sunlight, play a dominant role in initiating these reactions (Calvert et al., 2002; Altshuller, 1989). SOAs are a major component of fine particulate matter (PM) and are associated with significant health and climate impacts (Ju et al., 2022; Lelieveld et al., 2015; Li et al., 2022; Pope and Dockery, 2006). Understanding SOA formation is therefore essential for effective air quality management.

To understand the nature and sources of SOAs, source apportionment studies play a crucial role due to the vast diversity of VOCs emitted from both anthropogenic and biogenic sources (Claeys and Maenhaut, 2021; Dal Maso et al., 2016). These studies quantify the contribution of SOAs to PM concentrations and identify their origin, with urban measurements indicating that SOAs can account for up to 40% of PM_1 (Brines et al., 2019; Carlton et al., 2009). Controlled experiments using oxidation chambers and oxidation flow reactors (OFRs) are widely used to investigate SOA formation (Kang et al., 2007; Lambe et al., 2011; Surratt et al., 2006). Chamber studies allow the isolation of key parameters such as relative humidity (RH), nitrogen oxides (NO_x), and OH levels, while OFRs simulate atmospheric oxidation over shorter timescales; however, both approaches may not fully represent real atmospheric conditions. A key metric derived from these studies is the SOA yield, defined as the ratio of formed SOA mass to reacted VOC mass, which quantifies the

* Corresponding author.
E-mail address: leon@auth.gr (L. Ntziachristos).

https://doi.org/10.1016/j.apr.2026.103096
Received 11 October 2025; Received in revised form 8 June 2026; Accepted 8 June 2026
Available online 10 June 2026

efficiency of SOA production.

Several factors influence the formation of SOAs. Studies have shown a clear trend of increasing SOA yield with decreasing NO_x concentrations (Brégonzio-Rozier et al., 2015; Ng et al., 2007a). Branched structures of VOCs can further reduce yield, particularly under conditions of high NO_x concentrations (Lamkaddam et al., 2017; Loza et al., 2014). Temperature (T) also plays a role with cold conditions generally leading to higher SOA yields (Kim et al., 2012; Zhou et al., 2019). The influence of RH on SOA formation is complex and depends on the precursor and formation pathway. While several studies report reduced SOA yields under higher RH conditions compared to drier environments (Jia and Xu, 2018; Zhang et al., 2015) others have shown that higher humidity can increase SOA formation because water in aerosol particles can absorb water-soluble oxidation products and promote additional chemical reactions, resulting in greater particle mass formation (Pye et al., 2017). It is important to note, however, that some studies suggest a minimal impact of humidity (Dommen et al., 2006; Nguyen et al., 2011).

SOA formation models are commonly used to simulate secondary organic aerosol production. One widely used approach is the Volatility Basis Set (VBS) model, which simulates the partitioning of semi-volatile and intermediate-VOCs (S/IVOCs) between the gas and aerosol phases (Sasidharan et al., 2023) but relies on empirically fitted volatility bins and indirect representation of environmental dependencies (NO_x, T, and RH), without explicitly resolving chemical reaction pathways. In contrast, our approach uses GECKO-A yields which includes detailed multi-generational oxidation chemistry under multiple atmospheric conditions and precursor-resolved SOA trends. On the other hand, semi-explicit chemical mechanism models are employed, incorporating full chemical reactions for VOC oxidation and SOA formation (Eluri et al., 2018). The primary limitation of this approach is its computational cost, which can be substantial due to the complexity of the chemical mechanisms involved. In this study, we develop SOMA (Secondary Organic Module for Aerosol), a computationally efficient SOA formation approach using an oxidation equation to estimate SOA generation from VOC oxidation. This model incorporates key variables such as NO_x levels, SOA yields, oxidation duration, and OH concentrations specific to the environment being studied. The GECKO-A model is used for the calculation of the SOA yields used. Additionally, correction factors based on experimental SOA formation data from literature are used to account for the effects of other influential factors, such as RH, Tas well as other oxidants like O_3. SOMA applies regression-based correction factors to SOA yields, is calibrated with experimental data for accuracy, assumes irreversible partitioning for short-term formation, and provides a transparent, computationally efficient framework suited for Computational Fluid Dynamics (CFD)-based urban air quality studies.

Urban environments are hotspots for VOC emissions, originating from anthropogenic sources like traffic and households. These VOCs act as precursors to SOA and increase fine PM concentrations, adding to health concerns (Couvidat et al., 2013). Quantifying the dynamics of SOA formation in urban settings is a complex task due to the interplay between pre-existing SOA and unoxidized VOCs with SOA-forming potential. Studies have shown that using traditional chemical transport models accounting for primary VOC emissions can only quantify around 35% of observed SOA mass concentrations (Hodzic et al., 2009). More recent studies continue to report significant underestimation of SOA concentrations compared to observations mainly due to challenges in representing chemical aging, VOC oxidation pathways, and aqueous-phase SOA formation processes (Poupkou et al., 2025; Wu et al., 2025) and also cannot provide high spatial resolution of SOA concentrations (Jiang et al., 2012; Li et al., 2025).

The residence time of some VOCs can range from hours to days, (Ehn et al., 2014), and the recirculation of these compounds in urban environments can contribute to SOA production. To our knowledge, no study has quantified the contribution of background and local SOA at high spatiotemporal resolution in urban environments using CFD-based dispersion modelling. This gap arises from several key limitations such as the fact that chemical transport models typically operate at coarse spatial resolutions and cannot resolve street-scale variability, while CFD models, although capable of resolving complex urban flow and pollutant dispersion, generally neglect detailed atmospheric chemistry due to the high computational cost associated with simulating multi-generational oxidation processes. As a result, the coupling of detailed SOA chemistry with high-resolution CFD frameworks remains challenging, particularly when attempting to represent both local emissions and regional background contributions consistently (Baklanov and Zhang, 2020; Kadaverugu et al., 2019). To address this challenge, we propose a combined modelling approach that uses SOMA in CFD for high resolution pollution estimations for a highly trafficked area of the city of Augsburg, Germany. CFD air quality modelling is a well-established approach for assessing pollution levels, particularly at street scale (Boikos et al., 2024a; Du et al., 2021; Ioannidis et al., 2024a; Jeanjean et al., 2017). CFD accurately resolves turbulent flow and high-resolution pollutant fields, and here is used to provide realistic inputs to SOMA, rather than explicitly simulating complex SOA chemistry, which remains highly challenging and largely unexplored in urban CFD studies. The integration of SOMA with CFD enables high-resolution simulation of SOA dynamics in urban environments and provides a novel framework to quantify local and background contributions.

2. Methods

2.1. GECKO-A model

GECKO-A is a chemical mechanism generator capable of handling a large number of species and reactions. It is supported by the National Center for Atmospheric Research (NCAR) in the United States and the French Laboratoire Inter Universitaire des Systèmes Atmosphériques (LISA) (Aumont et al., 2005; Camredon et al., 2007). GECKO-A is designed to generate nearly explicit gas-phase oxidation mechanisms for one or more organic compounds under a range of atmospheric conditions. The model provides an online output library that serves as a comprehensive resource for researchers investigating SOA formation, offering data for over 50 different VOCs (Lannuque et al., 2018). A core capability of GECKO-A is its ability to calculate SOA yields of various organic compounds under controlled conditions. The concept of SOA yield plays a critical role in understanding the formation of SOAs during atmospheric reactions. The SOA yield is a dimensionless quantity, expressed as a ratio, often calculated over a specific time interval. It essentially reflects the potential of a VOC species to produce secondary aerosol while it oxidizes. It is defined as the ratio of the mass of SOA mass formed (SOA) to the mass of the reacted VOC (Equation (1)).

$$Yield = \frac{SOA}{\Delta VOC} \tag{1}$$

The GECKO-A model produces SOA yields for five distinct NO_x concentration levels, corresponding to remote (0.002 ppb), remote continental (0.0025 ppb), continental (5 ppb), polluted continental (20 ppb) and urban (200 ppb) environments (Camredon et al., 2007). Users can select a specific VOC and a NO_x pollution scenario, and then visualize how SOA yield changes over time, with temporal resolution ranging from seconds to hours. The SOA yields given by GECKO-A correspond to constant conditions of T at 25°C, (O_3 concentration of 40 ppb and RH at 70% (Camredon et al., 2007).

Fig. S1 of SM shows trends in SOA yields from toluene (C_7H_8), limonene ($C_{10}H_{16}$), isoprene (C_5H_8) and α-pinene ($C_{10}H_{16}$) under urban conditions (NO_x = 200 ppb) generated by GECKO-A, as examples. These compounds are selected due to their environmental significance and prevalence in experimental research studies (Ahmad et al., 2017; Bell et al., 2022; Brégonzio-Rozier et al., 2015; Oliva et al., 2023). For toluene (Fig. S1a), SOA yield exhibits a sharp initial increase, stabilizing

at around 0.6%, suggesting a balance between formation and loss processes influenced by NO_x levels (Ng et al., 2007a). In contrast, limonene (Fig. S1b) and α-pinene (Fig. S1d) show high initial yields (~20% and ~12% respectively) that decrease over time, likely due to fragmentation of highly oxidized products (Cain et al., 2021). Isoprene (Fig. S1c) presents a transient peak at 3%, declining rapidly to zero due to the quick fragmentation of its products, especially under high NO_x conditions. These trends highlight the significant role of precursor reactivity and oxidation mechanisms in SOA formation and how SOA yields can vary through time. It should be noted that the SOA yield profiles shown in Fig. S1 are derived from GECKO-A simulations performed at a fixed initial VOC concentration (1 pptvC). GECKO-A includes multigenerational oxidation chemistry in the generation of these yields; therefore, the temporal behavior reflects both precursor reactivity and the evolution of oxidation products under the simulated conditions. The observed decrease in SOA yield for highly reactive compounds such as limonene, isoprene, and α-pinene is also influenced by rapid precursor depletion under the assumed conditions.

A key limitation of predicted GECKO-A SOA yields is that parameters like RH, and T and oxidants like O_3 are held at reference values, which limits its use in real urban pollution simulations. Additionally, the model offers only five predefined NO_x scenarios, limiting its flexibility in representing the wide range of atmospheric NO_x concentrations observed in real-world environments.

2.2. SOMA development

2.2.1. SOMA architecture

SOMA calculates the formation of SOAs using a general approach based on the rate of an oxidation reaction (Equation (2)). This equation follows first-order reaction kinetics and is commonly used in atmospheric chemistry to model how VOCs react with OH (Chan et al., 2009). This equation incorporates the initial concentration of VOC and the rate of consumption, described through an exponential term that factors in the concentration of OH, the reaction rate constant between the OH radical and the precursor (k_{OH}) (Han et al., 2018; Singh and Li, 2007), and the oxidation period (Δt). The SOA yield (Y) of the specific compound for the given time is taken from GECKO-A.

$$SOA = [VOC] \cdot \left(1 - e^{-kOH \cdot [OH] \cdot \Delta t}\right) \cdot Y \quad (2)$$

This approach does not account for the influence of T and RH, factors that affect the formation of SOA and other oxidants like O_3. To address this limitation and improve the model's reliability, we introduce a correction factor (λ_{cor}) into the equation (Equation (3)). This factor is produced by collecting experimental information, as shown in Fig. 1, for every investigated compound to determine the influence of other parameters (O_3, T, and RH), given that the yields taken from GECKO-A assume constant conditions with O_{3gecko} = 40 ppb, T_{gecko} = 25°C and RH_{gecko} = 70% as explained in section 2.1. The parameterization of the new variables introduced is done by calibration with experimental data as will be elaborated in later section.

$$SOA = [VOC] \cdot \left(1 - e^{-kOH \cdot [OH] \cdot \Delta t}\right) \cdot Y \cdot (\lambda_{cor}) \quad (3)$$

2.2.2. Parametrization based on NOx concentrations for SOA yield selection

The five distinct NO_x scenarios explained in section 2.1 can be used to account for SOA yields at any NO_x level by interpolating between the data. Fig. 2 shows the SOA yield for the four species examined at a specific time selected (time = 1 h) for the five NO_x scenarios. Fig. 2a–d showcase high SOA yield at low-NO_x levels, at remote (0.002 ppb) and remote continental (0.0025 ppb) NO_x scenarios. Fig. 2c and d shows that the continental scenario (5 ppb) has higher SOA yield than the polluted continental (20 ppb), for limonene and α-pinene. Fig. 2a and c shows that the SOA yield is higher at the polluted continental scenario compared to the continental one for toluene and isoprene, but with minimal differences. In all cases, the high-NO_x scenario (200 ppb) demonstrates the lowest SOA yield.

The curve following the logarithmic fitting of the five points shows a decreasing trend with increasing NO_x concentrations (Pullinen et al., 2020). At low-NO_x environments, VOC oxidation typically proceeds through pathways that favor the formation of low-volatility compounds, which can readily partition into the aerosol phase, leading to higher SOA yields. In high-NO_x conditions, the oxidative processes tend to shift towards pathways that result to higher-volatility products, thereby suppressing SOA formation. The fitting curve allows us to calculate the SOA yield of any given time-period, for any NO_x level. This interpolated fitting curve allows us to estimate SOA yield values at any NO_x level without rerunning the GECKO-A model, which is necessary since we do not have access to the GECKO-A code but only to its published yield output library.

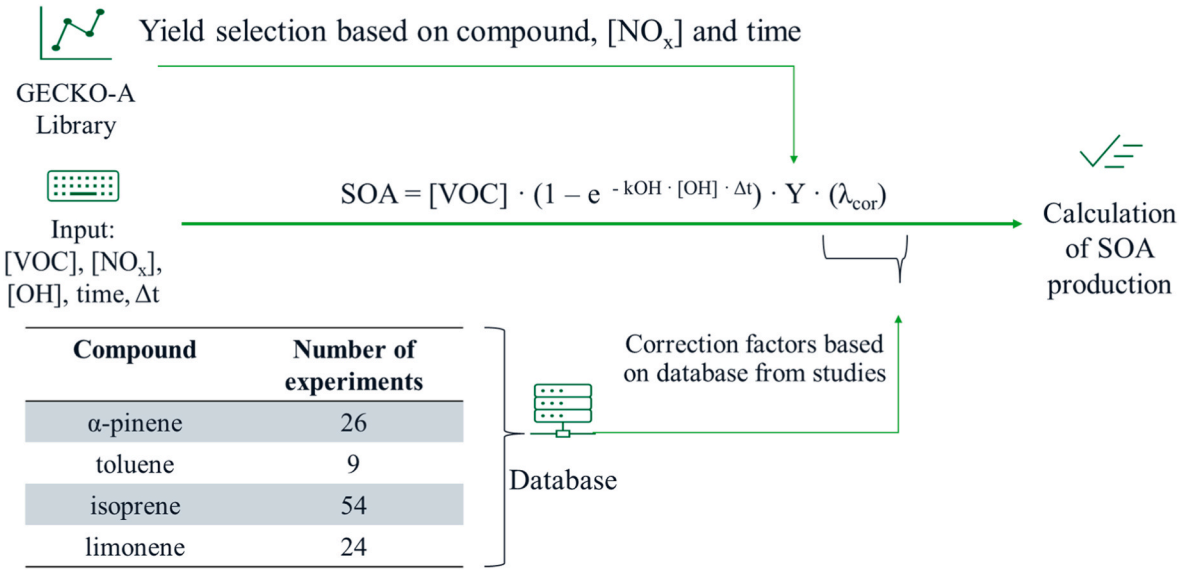

Compound	Number of experiments
α-pinene	26
toluene	9
isoprene	54
limonene	24

Fig. 1. SOMA uses [VOC], [NO_x], [OH], time and Δt as an input to calculate the amount of SOA generated. SOA yields are selected from the GECKO-A output library. The model uses correction factors accounting for the influence of O_3, T and RH based on experiments.

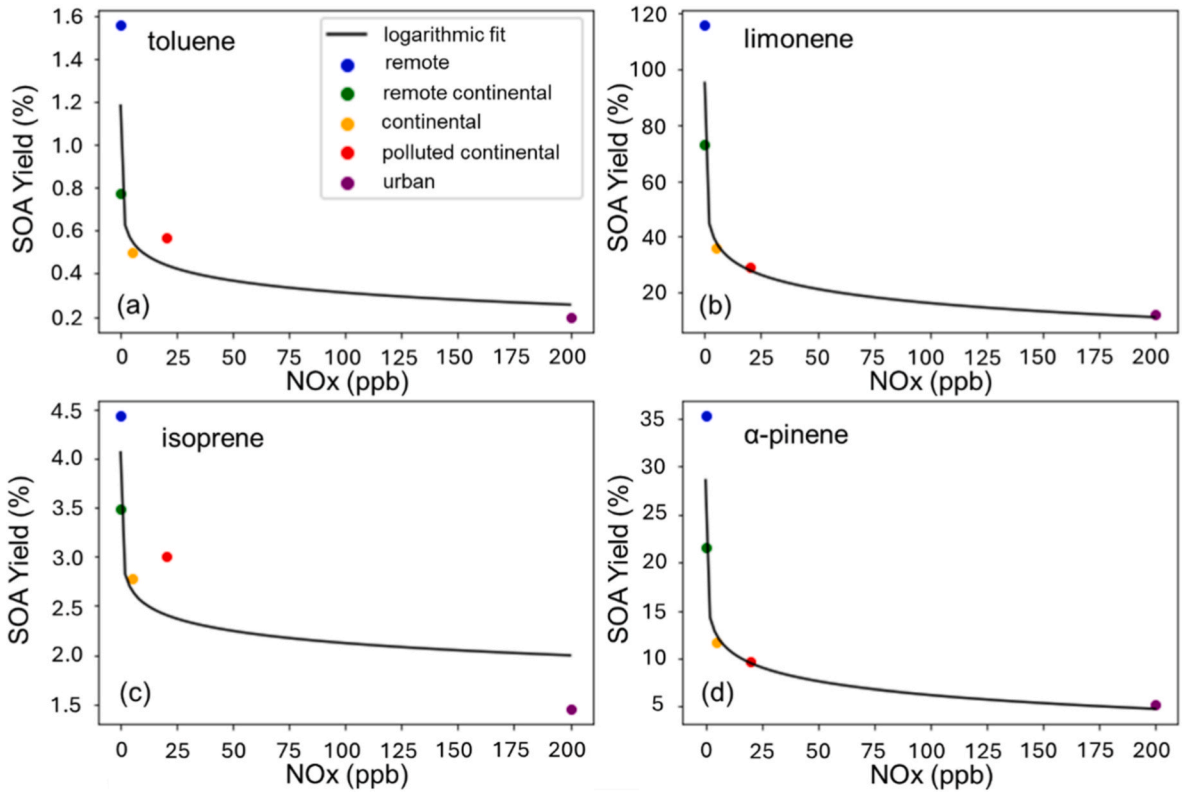

Fig. 2. SOA yields for 5 different NOx scenarios at 1 h, as generated by the GECKO-A model: remote (0.002 ppb), remote continental (0.0025 ppb), continental (5 ppb) polluted continental (20 ppb) and urban (200 ppb) for the four VOCs examined.

2.2.3. *Experimental data for SOMA calibration*

To validate SOMA and to provide reference for calibration, we gathered experimental information on the four mentioned VOCs in section 2.1. The selected experimental studies were limited to those that provided all required variables: VOC concentration, reaction time, NO_x, O_3, RH, T, OH concentration, and final SOA mass. This was necessary because our modelling approach with SOMA uses these specific environmental and chemical parameters as direct inputs to simulate SOA formation. Without complete documentation of these conditions, the experiments would not be suitable for generating accurate model inputs or for evaluating model performance. For example, Table S3 of the SM shows the data collected from two experimental studies, from 9 experimental measurements in total for toluene. In (Deng et al., 2017) the three experiments collected had a reaction time of 5 h, NO_x levels ranging from 68.2 to 72.2 ppb, RH from 50.5 to 55.5%, O_3 levels from 42.7 to 77.6 ppb and T ranging from 25.4 to 26.9°C. In (Chen et al., 2022) the reaction time of the experiments was 6 h, RH was set at 5% and NO_x levels ranged from 8 to 18.2 ppb. T and RH were constant throughout the experiments at T = 26°C and RH = 5%, and O_3 levels ranged from 54.9 to 94.6 ppb. Both studies were also selected because they did not include seed aerosol, in order to avoid uncertainties related to partitioning onto pre-existing OA. The data collected for every compound serve as reference for validation and as a base for experimental fitting based on the GECKO-A constant conditions to correct the SOA yields used by SOMA. All experimental data for toluene, isoprene, α-pinene and limonene is available at the Supplementary Material (S. M.).

2.2.4. *Experimental fitting of SOMA*

The developed SOA model generates the amount of SOA formed from oxidation of VOCs based on the chosen compound, the OH concentration, k_{OH} and the selected yield (determined by NO_x concentration and time). In the experimental fitting procedure, this process is repeated for every investigated compound, considering all the initial conditions from the experiments for the four compounds examined using the datasets explained in section 2.2.3. In the case that no information on OH concentration could be found, we assumed [OH] = 2×10^6 molecules/cm^3, typical of atmospheric conditions. The aim is to perform an analysis to determine the relationship between the ratio of SOA_{exp}/SOA_{orig} and the ratios of O_{3exp}/O_{3gecko}, T_{exp}/T_{gecko} and RH_{exp}/RH_{gecko}. The SOA_{orig} is the value the SOA model calculated using the initial conditions of the experiments without the introduction of correction factors and the SOA_{exp} is the value of SOA measurement given by each experiment. O_{3exp}, T_{exp} and RH_{exp} are the values taken from every experiment and the GECKO-A values are constant at O_{3gecko} = 40 ppb, T_{gecko} = 25°C and RH_{gecko} = 70%. By incorporating the experimental data, the correction factor produced enables the adjustment of the selected yields to better reflect the influence of varying environmental conditions. We note that this correction is empirical, not mechanistic, and is applied to bring SOMA's simplified yield predictions closer to observed chamber results given environmental variation.

Fig. 3a shows the regression graph between SOA_{exp}/SOA_{orig} and O_{3exp}/O_{3gecko}, T_{exp}/T_{gecko} and RH_{exp}/RH_{gecko} for the case of toluene (Table S3). Fig. 3a shows that for the case of O_3 the O_{3exp}/O_{3gecko} ratios ranged from 1 to 2.4 with an exception at 0.2, indicating that the experiments collected examined higher O_3 levels compared to GECKO-A O_3 levels. The T_{exp}/T_{gecko} ratios in all cases are very close to 1, as the temperatures examined in the experiments ranged from 25.8 to 26.9°C, and the GECKO-A temperature is considered constant at 25°C. As such, the influence of T is minimal in the toluene-specific dataset and any fitted temperature dependence here should be interpreted with caution. We include the T correction term in Equation (4) primarily to retain consistency across compounds, as in other VOC cases (SM) experimental temperatures vary more significantly and show a clearer influence on SOA yield. Thus, the regression method is designed to support multi-compound calibration and not solely optimized for toluene. The same

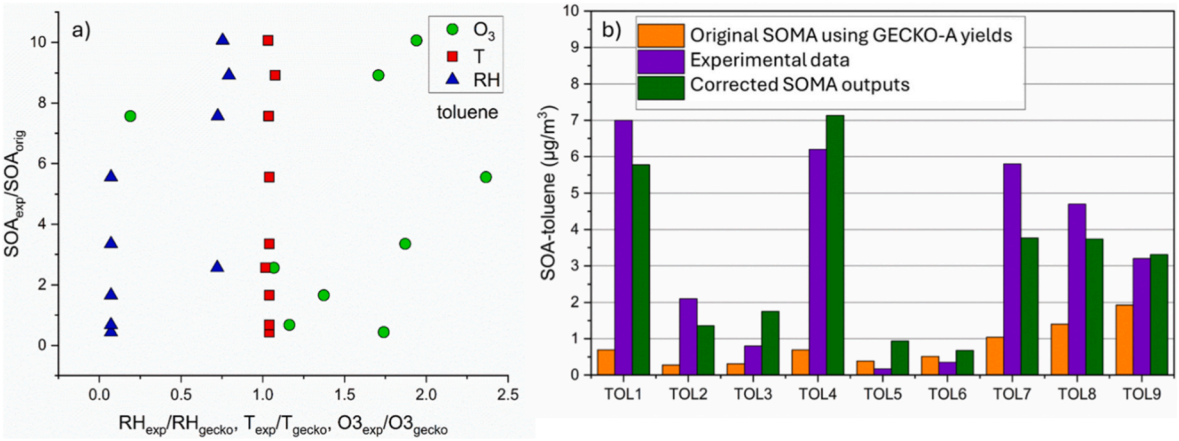

Fig. 3. Regression analysis of SOAorig/SOAexp with O3exp/O3gecko, Texp/Tgecko and RHexp/RHgecko based on the SOA formation experiments collected from literature for toluene (a). Comparison between experimental SOA concentrations, original GECKO-A estimates and SOMA predictions in the case of toluene (b). TOL1-9 represent the experiments of toluene SOA formation from Table S3 of SM.

analysis is performed for RH. The experimental RH used in the chamber studies was lower than the GECKO one with RH_{exp}/RH_{gecko} ratios ranging from 0.05 to 0.8. To account for the influence of the 3 variables examined we performed multivariable linear regression analysis to produce equation (4) that describes the influence of the ratios of the variables affecting SOA_{exp}/SOA_{orig}. For every set of experiment, we use the ratios of the variables in equation (4), to produce the SOA_{exp}/SOA_{orig} from the multivariable linear regression analysis. This ratio is then used to adjust the modelled value closer to the experimental one by multiplying the SOA_{orig} value.

$$\frac{SOA_{exp}}{SOA_{orig}} = -50.5 + 1.9 \times \frac{O_{3exp}}{O_{3gecko}} + 47.1 \times \frac{T_{exp}}{T_{gecko}} + 8.6 \times \frac{RH_{exp}}{RH_{gecko}} \quad (4)$$

Fig. 3b shows the comparison of the original SOA model's outputs and the corrected ones after the use of correction factors based on the influence of O_3, T and RH, with the corresponding experimental SOA concentrations. In all cases, the SOA_{exp}/SOA_{orig} ratio applied to the original model increased the calculated value, as it is evident that the original SOA model tends to underestimate SOA formation using the GECKO-A toluene yields. The original SOA model underpredicted experimentally determined SOA mass by 76% on average. Using the correction factors a 6% under-prediction across the average concentration is demonstrated in all studies. Taking into account all the corrections within the experimental fitting, we produced the λ_{cor} as a correction factor used in SOMA to account for the influence of O_3, T and RH in SOA formation. This correction factor is applied on the SOA yield. We acknowledge that additional nonlinearities, such as the dependence of SOA yield on existing organic aerosol (OA) concentration, are not explicitly treated in the current approach. Higher OA concentrations can enhance the partitioning of oxidation products into the particle phase, leading to increased SOA formation (Ng et al., 2007b). In this study, SOMA uses precomputed GECKO-A yield profiles generated under fixed conditions and therefore does not dynamically account for changes in OA concentration during simulations. As a result, SOA formation may be over- or underestimated under conditions with substantially different aerosol loadings. This simplification was adopted to maintain computational efficiency for high-resolution CFD applications and remains a limitation of the current approach. The same analysis for limonene, isoprene and α-pinene is shown in SM. It should be noted that the correction factors derived in this study are compound-specific and depend on the experimental conditions used for calibration; therefore, their direct application to untested VOCs is not recommended without additional fitting. Future development of SOMA could extend this approach to a broader range of compounds and parameters, enabling a more reliable calculation of SOA formation.

2.2.5. *Demonstration of NOx and OH influence on SOA formation*

After calibration, SOMA can be used to explore the impact of different parameters on SOA formation. Fig. 4 shows the influence of OH and NO_x on SOA formation within 1 h exposure of 1 µg/m^3 for toluene in typical atmospheric conditions. Fig. 4a demonstrates that within the range of specific OH levels (10^5 to 10^8 molecules/cm^3), the toluene SOA mass increases with increasing OH concentration (Sarrafzadeh et al., 2016). Beyond 2×10^8 OH molecules/cm^3, the SOA mass reaches a plateau, indicating a maximum yield and that additional increases in OH do not lead to further SOA production. Once OH radicals have oxidized all the precursors contributing to SOA formation, the remaining unoxidized precursors can no longer participate in SOA mass growth (Song et al., 2019). In this sensitivity analysis, conducted under fixed initial VOC loading, this behavior is primarily attributed to precursor depletion, as well as the absence of dynamically resolved multigenerational SOA formation in SOMA. In Fig. 4b, NO_x concentration exhibits an inverse relationship with SOA formation, aligning with the trends observed in the yield selection process from GECKO-A based on compound, NO_x concentration and time described in section 2.2.2 (Fig. 2). Fig. 4b reveals that within the range of 0.01 ppb to 500 ppb NO_x, SOA mass is inversely proportional to NO_x. This behavior can be attributed to the scavenging of radicals at high NO_x concentrations, thereby limiting oxidation and subsequent conversion of gas-phase precursors to the aerosol phase (Pullinen et al., 2020).

This approach for predicting SOA formation under specific environmental conditions shows strong potential for Air Quality (AQ) modelling applications. Estimated VOC concentrations can be input directly into SOMA. Using the VOC emission source data, the model can set the emission duration as the oxidation period. To reflect environmental influence, the model can also incorporate as an input NO_x and OH concentrations, whether measured or modelled. Additionally, the correction factors make the module more robust by accounting for other oxidants, like O_3, as well as environmental parameters that affect SOA formation, such as RH and T.

2.3. *Numerical model*

This study uses OpenFOAM, an open-source CFD code, to model pollutant dispersion from traffic within the chosen urban environment. For this work the steady-state simpleFoam solver, employing the Reynolds-averaged Navier-Stokes (RANS) approach, is used for calculating the velocity field (Boikos et al., 2024b; Peralta et al., 2014; Rapkos et al., 2024). The steady-state RANS approach is used because emission rates and meteorological conditions implemented as input to the CFD model concern hourly values and are considered constant for every

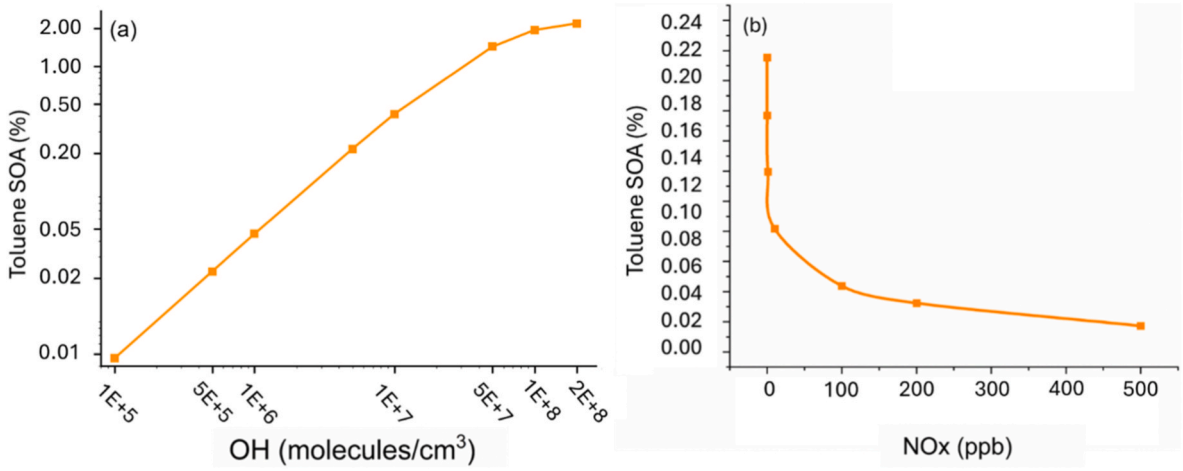

Fig. 4. Influence of (a) OH and (b) NO_x concentrations on SOA toluene formation, demonstrated by the SOMA model, by using initial concentration of 1 μg/m^3 of toluene for 1hr for every case.

hour.

$$\frac{\partial C}{\partial t}+\frac{\partial(\overline{u_j}C)}{\partial x_j}-\frac{\partial}{\partial x_j}\left(Dt\frac{\partial C}{\partial x_j}\right)=0 \tag{5}$$

$$Dt=\frac{vt}{Sct} \tag{6}$$

$$\boldsymbol{U(z)=\frac{u^*}{\kappa}ln\left(\frac{z+z_0}{z}\right)} \tag{7}$$

The advection-diffusion equation (Equation (5)) governs this transport process within the solver (Antoniou et al., 2024; Ioannidis et al., 2025; Miao et al., 2014). This equation includes the turbulent diffusion coefficient (Dt). Due to the dominance of turbulent diffusion, particularly in low-wind speed scenarios, the molecular diffusion term (Dm) that is sometimes used in CFD dispersion modelling can be safely neglected (Bonifacio et al., 2014; Rapkos et al., 2023). The turbulent Schmidt number (Sct) is used to calculate Dt (Equation (6)), with a recommended value of 0.7 (Tominaga and Stathopoulos, 2007). The k-ε turbulence model is chosen for its well-known effectiveness in simulating pollutant dispersion within urban environments (Pantusheva et al., 2022). The inclusion of Atmospheric Boundary Layer (ABL) profile (Equation (7)) at the inlet boundaries of the computational domain enhances the model's accuracy by capturing the characteristics of airflow within the urban landscape (Yang et al., 2009). These profiles are determined using friction velocity (u*), Von Karman constant (κ), and aerodynamic roughness length (z_0), providing a representative wind field behavior in urban settings. Detailed information of the numerical model setup can also be found in Table S1 of S.M.

2.4. Case study

This study focuses on Augsburg, Germany, a city in the Bavaria region. Fig. 5a provides a broader view of the city, while Fig. 5b zooms in on the specific area chosen for the computational modelling. This area is selected for its central location in the city. The case study area comprises of an official AQ monitoring station (Königsplatz KP) as shown in

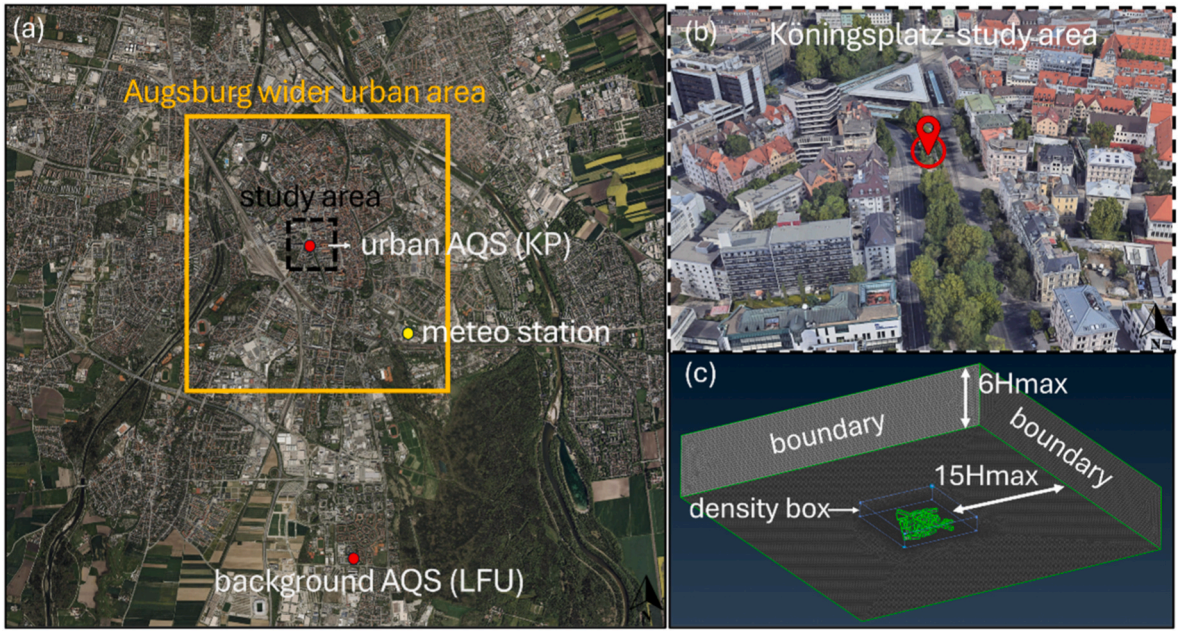

Fig. 5. Augsburg city area and focus on study area (a). Air Quality station placed on key position in the study area in Königsplatz (b). Computational domain and mesh development (c). © OpenStreetMap contributors 2024. Distributed under the Open Data Commons Open Database License (ODbL) v1.0.

Fig. 5b, operated by the Bavarian State of Environment, strategically placed between two main roads at a height of 4 m. It provides concentration measurements of pollutants like PM_{10}, NO_2, NO, CO, benzene, toluene and xylene. On the southern side of the study area, a background station (LFU) also provides pollutant concentration measurements for the same pollutants, indicating the regional background levels of Augsburg city. On the southeast side of the urban area, a meteorological station provides information of wind speed and wind direction on an hourly basis.

Representation of the urban environment's geometry is essential for reliable air quality modelling using CFD. This allows for precise predictions of pollution levels within the urban canopy (Trindade da Silva et al., 2021). To achieve realistic representation of the urban environment examined we obtained the 3D geometry of the study area from Open Street Maps (OSM). Following data acquisition, the building surfaces were processed to remove inconsistencies and enhance their definition. As illustrated in Fig. 5c, the digital domain extends beyond the immediate area. The distance between the study area and the computational domain's boundaries is set at 15 times the maximum building height (Hmax) and the height of the domain at 6Hmax, with the highest building in the area standing at 50 m (Table S2). This approach aligns with established practices (Blocken, 2015).

A computational grid that covers the study area was constructed. The volume mesh that covers all the domain uses tetrahedral unstructured elements which are irregularly arranged four-node volumetric cells that allow flexible representation of complex urban geometries (Hu et al., 2022). The resolution on the buildings shown in Fig. 5c is 1 m, on the emissions sources 0.25 m and on the boundaries of the domain 15 m (Table S1). Also, for high refinement around the buildings, a density box is developed as displayed in Fig. 5c that sets the maximum element size at 4 m allowing for high spatial accuracy of the CFD outputs with high refinement within street canyons and the sensor location. The computational grid consists of a total of 7 million elements. Mesh sensitivity analysis has been performed in previous studies performing CFD modelling in Augsburg city (Gkirmpas et al., 2024; Ioannidis et al., 2024a, 2024b), showing that this mesh resolution has acceptable convergence criteria with scaled residuals within the accepted range of $10^{-6} - 10^{-7}$ as proposed (Pantusheva et al., 2022).

2.5. Traffic emissions and meteorological conditions

The emission source setup (Fig. 6a) shows that in the study are we included 5 unique road IDs. Hourly deviations from the Annual Daily Traffic Volume (ADTV) for each road ID were produced for September 2018, resulting in a detailed hourly traffic activity profile (Ioannidis et al., 2024b). VOC emissions were calculated using COPERT Street software for the year 2018 in Germany based on the traffic activity. The vehicle classification considered: 73.6% passenger cars, 12.7% light commercial vehicles, 7.5% motorcycles, 5.6% heavy-duty trucks, and 0.6% buses as taken from the Federal Motor Transport Authority for the examined urban area in Augsburg. A total of 5 emission sources corresponding to the road IDs were integrated within the digital model, which simulate emission rates from the road segments in the modelling domain.

Meteorological data collected for September 2018, when the traffic data was available, revealed a prevailing south-westerly wind direction with an average speed of 0.90 m/s, with maximum wind speed observations at around 4 m/s as seen in Fig. 6b. The meteorological station that this data was obtained from is positioned on the southeastern side of the wider Augsburg area (Fig. 5a), specifically chosen to minimize the influence of the urban landscape on wind observations. A 24-h period was chosen that exhibited a dominant south-western wind direction, with an average wind speed of 0.82 m/s, during 11/09/2018, to perform simulations for pollutant dispersion. This selection reflects the prevailing characteristics of the data collection period, ensuring that the results obtained are representative. Toluene is selected as the compound of interest, as this is primary emitted from traffic activity (Mehta et al., 2020) and its concentration measurements are available from the Air

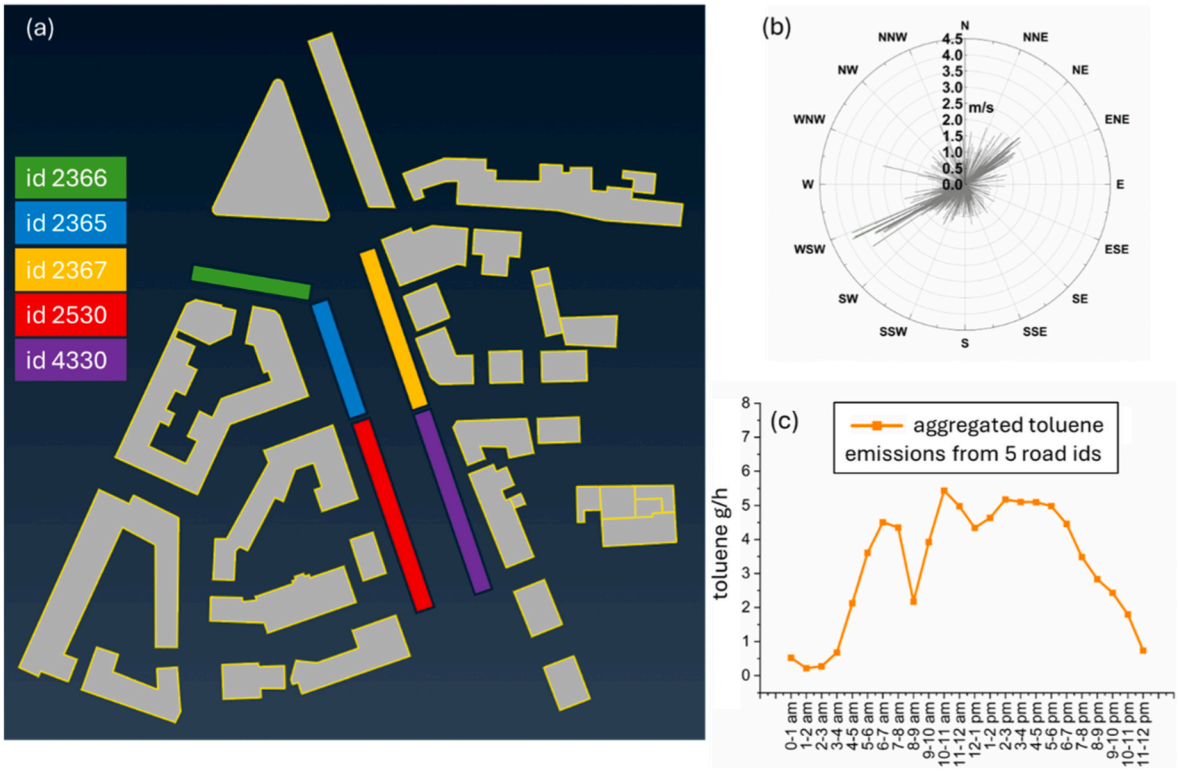

Fig. 6. Emission sources placed on road representing traffic activity (a). Rose graph of observed wind speed and direction during September 2018 in Augsburg (b). Total toluene emissions from traffic from all the road IDs (c).

Quality station in our study area. Toluene emissions are estimated as a fraction of total VOC (Huang et al., 2020), calculated by the COPERT model. Fig. 6c depicts the total emitted mass of toluene during the selected period for the 5 road IDs included in the model with distinguishable day and night emission profiles in the examined period, typical for urban driving volumes.

2.6. CFD simulations using street and background sources

The CFD model developed for this study is used to produce pollutant concentrations from street and background sources. To save computational time, CFD simulations of distinct meteorological scenarios are performed, using 8 wind directions with an angle increment of 45°, for 2 sets of wind speeds, at 1 m/s (low) and 3 m/s (high). Running distinct wind scenarios to save on computational time has been effectively used to produce pollutant concentrations with CFD modelling in other studies (Boikos et al., 2025; Rivas et al., 2019). Simulations are performed for two different conditions. By only considering traffic emissions by the emission sources explained in Fig. 6a, and by considering background concentrations on the boundaries of the computational domain, shown in Fig. 5c. For traffic emissions, the concentration $C_{source,\ street}$ was set as boundary condition in the CFD model setup on the grid corresponding to the emission sources specified in Fig. 6a, calculated from emission releases in Fig. 6c. For background sources, the initial concentration $C_{source,\ background}$ represents pollutant concentrations in neighboring areas, set as boundary concentrations on the computational domain. By dividing the simulated concentrations in points of interest with the initial concentration at the boundaries or at the emission sources, we can determine the dimensionless value of the concentration ratio (CR) according to the distinct meteorological scenario examined (WD, WS). The concentration ratios for traffic and background contribution are defined in Equation (8).

$$CR_i = \frac{C_{point}}{C_{source,i}} \tag{8}$$

Where i stands for 'source' or 'background'. To account for wind conditions not explicitly simulated in the CFD model, a linear interpolation function was used to estimate the concentration ratio for any observed wind speed (WS_{real}) and direction (WD_{real}), shown in Equation (9). The CFD simulations were performed for a discrete set of meteorological scenarios consisting of 8 wind directions (with 45° increments) and 3 wind speed classes. For any observed wind condition falling between these predefined scenarios, the concentration ratio was obtained through linear interpolation between the nearest simulated wind directions and speeds. Specifically, the method interpolates between the four surrounding CFD cases (two wind directions and two wind speeds), providing a continuous estimate of the dilution factor across the meteorological space.

$$CR_{real,i} = f(WD_{real}, WS_{real}) \tag{9}$$

The pollutant concentration at any point of the domain can be calculated depending on the contribution of each source type. The pollutant concentration produced by the CFD model from street or background sources can be calculated using equation (10):

$$C_{point,i} = C_{source,i} \times CR_{real,i} \tag{10}$$

This methodology allows for the calculation of pollutant concentrations under varying meteorological conditions. A limited set of CFD simulations produces any pollution scenario using wind data based on real observations. For this work, we used a total of 32 sets of simulations (8 wind directions × 2 wind classes × 2 sources). The use of simulations of different pollution origins allows the identification and quantification of contributions from street and background sources. We name the interpolation functions as $fCFD_{street}$ and $fCFD_{background}$ from now on to represent the usage of the CFD model to calculate concentrations from street and background sources respectively on any selected point.

3. Results

3.1. CFD model validation

The validation of the CFD model was achieved by comparing simulated toluene concentrations from street emission sources with measurements obtained from the KP urban traffic hotspot station. Toluene was chosen because it is the only SOA precursor that can be directly linked to traffic in a city environment for which actual concentration measurements were available. Following the methodology explained in section 2.6 by using traffic emissions and meteorological data for the selected daily period, we produced gaseous toluene concentrations at the point of the Air Quality station, within the digital domain. CFD concentration predictions were incrementally added to toluene concentrations measured at an air quality station outside of the city (LFU station - Fig. 5a), that served as the background. This approach assumes a uniform background concentration within the modelled domain to account for the impact of sources not related to urban emissions (Tchepel et al., 2010). Given the moderate atmospheric lifetime of toluene and the limited spatial extent of the domain, this assumption is considered reasonable over the modelled time period. The LFU background station is located away from direct traffic influence and provides stable background values that we superimpose with CFD-simulated traffic concentrations to reconstruct total levels at the KP station. Fig. 7 demonstrates good agreement between measured (black curve) and estimated toluene concentrations (orange and striped green columns) over a 24-h period, with an average deviation of 8% and a correlation coefficient of 0.83. Fig. 7 also depicts the NO_x concentration measured during the chosen period at the KP station, showcasing the highest peak around 06:00-08:00 corresponding to the morning rush hour associated with traffic activity, the primary source of NO_x. Hourly NO_x levels within the investigated area were used as input for the SOMA to calculate the corresponding SOA yield, as detailed in section 2.2.2.

In this section we also performed direct comparison of CFD generated toluene concentrations that are attributed to only traffic activity. To do that we identified the part of the measured toluene concentration that could be attributed to traffic activity. By subtracting the corresponding toluene concentrations measured at the background station (LFU) located on the southern side of the urban area for the same hour from the measurement at KP, we can determine the street increment of the measurement. This is indicated by the green curve in Fig. 7. The CFD generated toluene concentrations over the day, as shown by the striped green bars. These exhibit distinguishable peaks during morning and

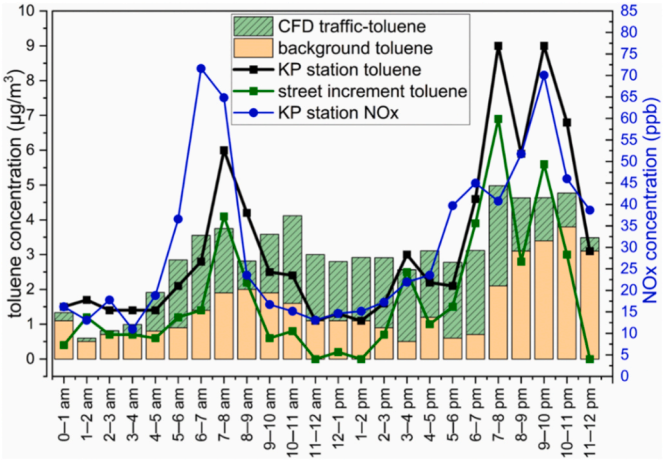

Fig. 7. Comparison of measured and estimated toluene concentrations at the location of the air quality sensor, together with measured NOx concentration.

afternoon periods. The same trend can be seen following the green curve of the street increment of measured toluene. The average daily concentration of street increment during this period was 1.75 μg/m^3. When using only traffic emissions as input, the CFD model produced average daily toluene concentration of 1.50 μg/m^3, closely matching the observed street increment, producing values within the same range as measurements. While the hourly comparison showed some negative increments—due to instances when the background measurement was higher than the KP station measurement (between 11 and 12 a.m. and 1−2 p.m., as shown in Fig. 7)—the daily concentrations obtained from both the CFD model, and the street increment, meaning comparing the green curve and the striped green bars, showed a deviation of 15%. The agreement with measured toluene concentrations suggests that the model effectively replicates the dispersion of traffic-related toluene within the urban environment, especially if one considers uncertainties of exact traffic rates and emission factors related to the calculation of total emission rates.

3.2. SOA estimates

3.2.1. Coupling SOMA with CFD

The temporal resolution of available wind data and emission rates was hourly, so CFD derived concentrations were also of hourly resolution. In urban environments, the OH levels vary between 0.7 and 8 × 10^6 molecules/cm^3 depending on light intensity, temperature and the presence of certain pollutants (Cho et al., 2023). No information on urban OH levels was available for this study, so we selected an OH concentration of 2 × 10^6 molecules/cm^3. This value falls within the lower-middle range of typical OH concentrations reported in urban studies (Zou et al., 2023) and reflects representative daytime conditions in polluted environments. The sensitivity analysis shown in Fig. 4a for toluene used multiple OH values, with 10^6 and 5 × 10^6 molecules/cm^3 lying within the range reported for urban atmospheric conditions. Relative to the selected OH concentration, these values resulted in variations in predicted SOA formation of approximately a factor of 0.4 to 1.8. This demonstrates that uncertainty in OH concentration can affect predicted SOA concentrations. However, the selected OH value lies within the range commonly reported for polluted urban environments and provides a reasonable estimate for the present study. We used a conservative estimate to avoid overestimating SOA formation, given the absence of direct OH measurements in Augsburg. VOC to SOA conversion was predicted by means of eq. (3). Where VOC concentrations were produced by the CFD for the different cells of the domain, assuming only toluene.

3.2.2. Pollutant recirculation approach

Certain VOCs can remain in the air for hours to days, allowing them to recirculate in urban areas and contribute to SOA production. This contribution often originates from neighboring areas and can accumulate over various time scales. To estimate the contribution of SOA originating from neighboring areas to the study domain, we assume that traffic patterns are consistent throughout the broader urban region due to similar driving conditions of urban environments. This assumption was supported by the fact that the modelled domain lies centrally within Augsburg and is surrounded by areas with comparable land use, emission sources, and road networks. By focusing on our specific case-study area, we argue that traffic-related emissions can be considered representative of the surrounding zones, given the study area's central location within the city of Augsburg (Fig. 5a).

SOA from neighboring areas could manifest itself in the modelling domain in two ways. First, as transported SOA formed in previous time frames outside of the modelling domain and getting diluted through time, as it is transported to the modelling domain. Second, from previously emitted VOC that is transported to the modelling domain and forms fresh SOA within the domain of interest. To clarify, SOA in the modelling domain can have three different origins:

1. Freshly formed SOA resulting from VOC emissions produced within the domain during each hour modelled. This is referred to as fresh SOA **(F-SOA).**
2. Previously formed SOA outside of the modelling domain, transported into the study area within the given hourly time frame, referred to as background SOA **(BG-SOA).**
3. Freshly formed SOA resulting from VOC transported into the modelling domain from neighboring areas, referred to as background fresh SOA **(BGF-SOA).**

We group BG-SOA and BGF-SOA together as "background SOA," representing all non-local contributions to total SOA during each hourly period. This recirculation approach allows us to estimate background and delayed SOA contributions using only local emission and meteorological data, without requiring external boundary condition inputs. This enables clear differentiation between fresh and recirculated SOA mass, as defined by the F-SOA, BG-SOA, and BGF-SOA categories. Equation (11) is used to calculate the total SOA mass concentration.

$$\mathrm{SOA}total = (\mathrm{F-SOA}) + (\mathrm{BG-SOA}) + (\mathrm{BGF-SOA}) \quad (11)$$

The representation of the approach used to calculate local and background contribution to simulated SOA concentrations is shown in Fig. 8. Fig. 8a shows that fresh SOA (F-SOA) for each time period is calculated using VOC concentrations generated by the CFD street emission modelling. For each hourly period, the CFD model estimates VOC concentrations produced by local street emissions and SOMA estimates F-SOA concentrations.

By using the CFD generated toluene concentration fields from street emissions, we can also calculate the average VOC concentration in the whole domain, by calculating the concentration of every point of the grid. We then implement the domain VOC concentration in SOMA, to calculate the SOA formed in our case study area (equation (12)) and VOC consumption given by the term ΔVOC (equation (13)). The remaining unoxidized VOC ($\mathrm{VOC_{remaining\text{-}domain}}$) amount after can then be calculated using equation (14).

$$\mathrm{SOA_{domain}}\,[t-1] = fSOMA\backslash(\mathrm{VOC\_(domain)}\,[t-1]\backslash) \quad (12)$$

$$\Delta\mathrm{VOC\_(domain)}\,[t-1] = [\mathrm{VOC\_(domain)}\,[t-1]\cdot\left(1-e^{-\mathrm{kOH}\cdot[\mathrm{OH}]\cdot\Delta t}\right) \quad (13)$$

$$\mathrm{VOC_{remaining-domain}}[t-1] = \mathrm{VOC_{domain}}\,[t-1] - \Delta\mathrm{VOC_{domain}}[t-1] \quad (14)$$

The terms $\mathrm{SOA_{domain}}$ [t-1] and $\mathrm{VOC_{remaining\text{-}domain}}$ [t-1] represent the average SOA formed and remaining VOC in the domain respectively as calculated by equations (12) and (14) for time [t-1]. These two terms are then used as input to the CFD simulations of background sources for the next time period (t) as illustrated in Fig. 8b. They represent pollutants present in the domain of interest from neighboring areas, assuming similar traffic activity in both environments. We assumed that similar emissions and meteorological conditions in the broader urban setting lead to comparable VOC and SOA levels in the surrounding areas, justifying their use as boundary input. The CFD background model calculates the concentration of already formed SOA at the point of KP station introduced as background, based on the meteorological conditions of time t. The concentration calculated is denoted as BG-SOA.

$$\mathrm{BG-SOA_t} = fCFD_{background}(\mathrm{SOA_{domain}}[t]) \quad (15)$$

The CFD dispersion model is then used to calculate the VOC concentration at the point of KP station, from background remaining unoxidized VOC. The $\mathrm{VOC_t}$ concentration can be calculated by equation (16), using meteorological conditions of the corresponding period.

$$\mathrm{VOC_t} = fCFD_{background}\left(\mathrm{VOC_{remaining-domain}}[t]\right) \quad (16)$$

The SOA formed from VOC presence during that time can be calculated by equation (17), using the environmental conditions of that time. This is now denoted as background fresh SOA (BGF-SOA).

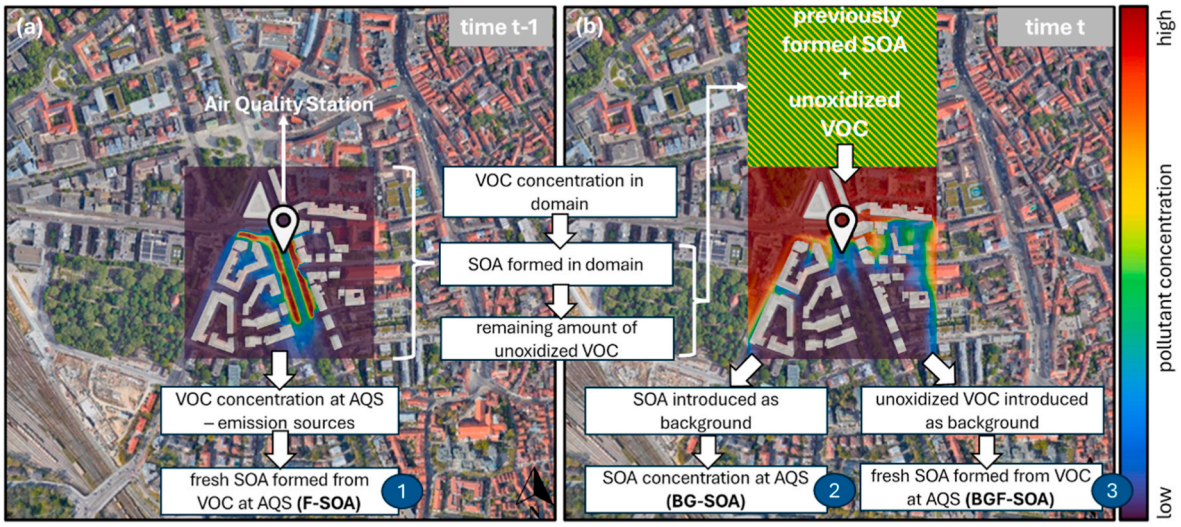

Fig. 8. Schematic representation of the approach for identifying fresh SOA (F-SOA) (a), background SOA (BG-SOA) and background fresh SOA (BGF-SOA) (b). © OpenStreetMap contributors 2024. Distributed under the Open Data Commons Open Database License (ODbL) v1.0.

$$\text{BGF-SOA}_t = fSOMA(\text{VOC}_t) \quad (17)$$

By repeatedly calculating the formation of SOA and consumption of the VOC we can use the combination of the SOA model and the CFD to calculate for every time period the amount of F-SOA, BG-SOA and BGF-SOA. At the end the total SOA concentrated at the point of interest, will be the sum of the three different SOAs calculated (equation (11)). The freshly produced SOA from street emissions at the corresponding time (F-SOA), the already formed SOA that is transported and diluted (BG-SOA) and the freshly produced SOA from background VOCs (BGF-SOA), simulating a pollutant recirculation effect within the urban environment. While intermediate oxidation products are not explicitly tracked during CFD runtime, multigenerational chemistry is represented implicitly through the precomputed GECKO-A yield profiles.

3.3. *Influence of local and background contribution to SOA concentrations using the pollutant recirculation approach*

To demonstrate the model's application in accounting for SOA formation, we selected a 12-h period (06:00−18:00) on the day examined, considering that sunlight is present during this period to initiate the photo-oxidation of toluene (Altshuller, 1989a; Li et al., 2021). In Fig. 9, each hour shows the contribution of SOA from toluene emissions, starting from the initial analysis at 06:00. For instance, SOA formed from toluene emissions from traffic between 07:00 and 08:00 makes up 79% of the SOA mass during that time, representing fresh SOA (F-SOA) formed from recent emissions. The remaining 21% of the SOA mass has a background origin. This background portion includes SOA that had already formed from toluene emissions between 06:00 and 07:00 and has since diluted (BG-SOA), as well as additional SOA formed between 07:00 and 08:00 from toluene emitted during the earlier 06:00–07:00 period (BGF-SOA). Later in the day, for example, between 17:00 and 18:00, 47% of the SOA is produced locally from toluene emissions during that specific time, while the remaining 53% has background origins, resulting from emissions that occurred from 06:00 up until 17:00. Notably, less than 1% of the SOA concentration during this time can be attributed to emissions before 11:00–12:00, indicating minimal contributions from earlier emissions. To clearly distinguish local from background SOA contributions, striped slices are used to indicate locally formed SOA, while solid-colour slices represent background SOA contributions. The trend shown in Fig. 9 indicates that SOA contributions from toluene emissions at 06:00–07:00 steadily decline throughout the day until 18:00. This decline results from the progressive consumption and dilution of the toluene responsible for SOA formation, as estimated by the recirculation approach. Similar behavior is observed for toluene emissions at other times, where their contribution to SOA mass decreases through time.

This analysis allows us to assess the cumulative contribution of SOA formed over different timescales, helping to identify when older SOA formations have a negligible impact on current SOA concentrations. In Fig. 10, the SOA concentration at time = 0 represents locally formed, fresh SOA (F-SOA) for each period examined. For any given period, the total SOA originating from time = 0 corresponds solely to the freshly formed SOA. As time progresses, the total SOA in each period increases as SOA from prior time intervals is incorporated, adding background-originated SOA mass to the overall modelled SOA. In Fig. 10, the black curve illustrates the cumulative SOA concentration for the 17:00–18:00 period. Here, SOA originating specifically from 17:00–18:00 (i.e., time = 0 for this period) has a concentration of 1.53×10^{-3} μg/m^3, representing the local SOA formed during this time. Moving one step backward along the x-axis to time = −1 (16:00–17:00), the total SOA concentration increases to 2.22×10^{-3} μg/m^3 as SOA from the prior hour is added. This approach highlights how cumulative SOA concentrations evolve over time, illustrating how contributions from earlier time periods influence total SOA levels across examined timescales.

By continuing to account for the background SOA contribution to the total SOA mass concentration calculated, we can determine at what point this cumulation ceases to make significant difference to the total SOA concentration. Fig. 10 reveals that the contributions of SOA stabilize after 7 h, indicating that earlier background SOA generated by traffic has a minimal impact on current concentrations. This stabilization occurs because the VOCs emitted in earlier time periods have either been consumed through chemical reactions or broadly diluted in the atmosphere. As a result, after 7 h, the cumulative effect of background SOA becomes negligible. This 7-h threshold provides a useful estimate of the effective atmospheric memory of traffic-related SOA within the modelling domain. It suggests that, under similar urban conditions, the recirculation-based background contribution is most relevant within this timeframe and declines afterwards. Therefore, the recirculation approach used here may be applicable to other urban-scale studies, provided the city's emission dynamics and atmospheric conditions support a comparable chemical lifetime and dispersion behavior.

Our approach shows that although local contributions remain more dominant overall, the impact of total background SOA grows stronger

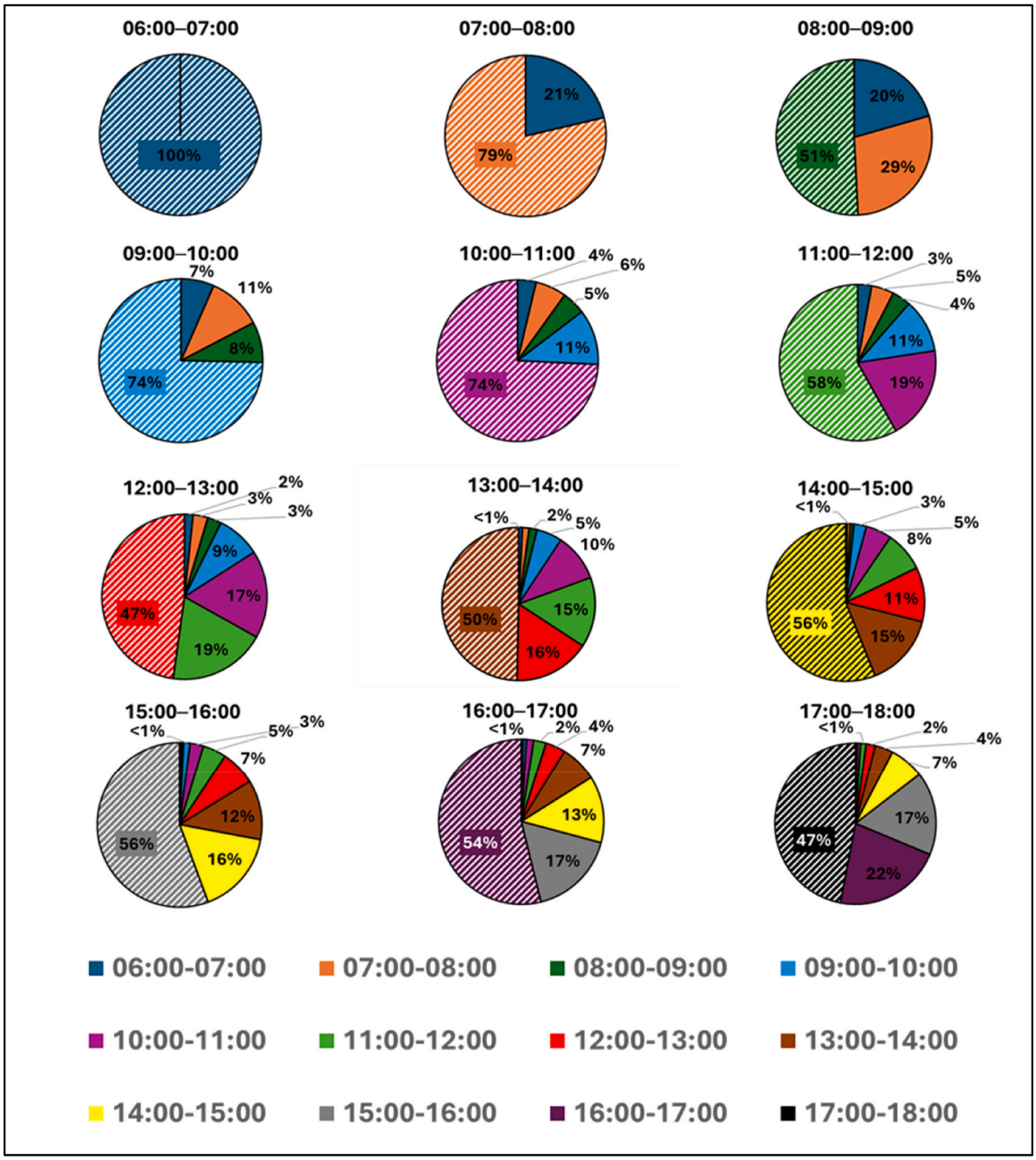

Fig. 9. Local (striped slices) and background contribution on SOA concentration from traffic-toluene emissions produced by recirculation approach.

over time due to the accumulation of previously formed SOA mass from multiple time scales. The findings of this work are specific to toluene, the VOC examined in this modelling approach. It is crucial to recognize that different VOCs may exhibit unique behaviors, and the background SOA from their oxidation could yield different results. Therefore, the conclusions drawn for toluene may not be directly applicable to other compounds, and each precursor's contribution to background SOA should be individually assessed. Nevertheless, toluene is a significant component of traffic emissions, making these conclusions broadly relevant for understanding traffic-related SOA formation in urban environments. Future research could expand this modelling approach by including various other primary emitted precursors to better understand the local and background effects on SOA formation over different timescales from dominant urban emission sources. Such insights are essential for developing effective policy measures to mitigate these pollutants, as they cannot be accurately quantified by simply correlating SOA presence with primary emissions.

4. Conclusions

SOAs are formed by the oxidation of VOCs and have an important contribution to fine PM concentrations. Understanding SOA formation is crucial as the high residence time of some VOCs, that ranges from hours to days, can contribute to SOA production. To capture the dynamic effect of SOA formation from traffic activity in urban areas we introduce SOMA a module that can be implemented in air quality modelling. SOMA uses an oxidation equation based on OH radical interactions with precursors and incorporates data such as VOC, OH and NO_x concentrations, oxidation duration, and specific oxidation rate constants. By analyzing 113 chamber experiments involving α-pinene, isoprene, limonene, and toluene, correction factors were established based on O_3, relative RH, and T influence on SOA production. The correction reduced

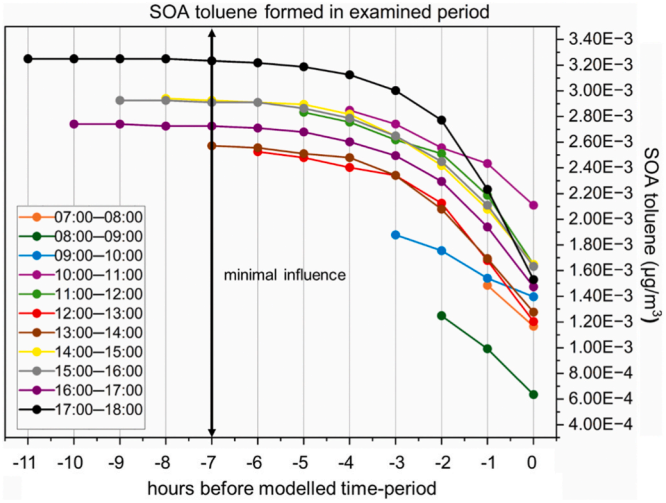

Fig. 10. Cumulative SOA concentration from traffic-toluene at the sensor location. The x-axis indicates how many hours ago the SOAs were formed and have an influence on SOA concentrations in every time-period.

deviations from experimental values.

To illustrate SOMA implementation in air quality modelling, a CFD model is developed to simulate toluene emissions from traffic in a high-traffic area of Augsburg, Germany. Simulations were used to calculate toluene concentrations from both street and background sources. The results of these simulations were used in a novel approach, reflecting recirculating pollution from neighboring areas influenced by meteorological conditions. The modelled toluene concentrations were validated against official air quality station measurements. SOA formation from CFD-generated toluene was examined over a 12-h period, considering atmospheric conditions and OH presence. A limitation of this study is that OH levels were assumed based on common urban conditions. Future implementation of SOMA in air quality models could benefit from actual OH trends observations in the examined environments for more representative results.

The modelling approach estimated the local and background effect on SOA formation from traffic in the examined area. SOMA and CFD coupling showed that SOA originating from toluene oxidation has diverse sources through time. During the 12-h period examined, focusing on the point of the air quality station of the area, the background SOA was 21-53% of identified SOA mass. Also, analysis has shown that after 7 h, the contribution of background SOA has negligible influence on the concentrations modelled. The recirculation effect of each precursor individually has strong influence up to 7 h and decreases due to the consumption and the dilution both of the SOAs and the VOCs. The results of this integration are based on toluene, but it's important to acknowledge that other VOCs may exhibit different SOA yields. Future development of SOMA could expand to include the full spectrum of VOCs from specific emission sources.

This study provides valuable insights into the formation and sources of SOAs, offering guidance for the scientific community to better understand SOA production from VOC emissions. As SOAs significantly affect air quality and human health, this research provides innovative modelling techniques that enhance air quality capabilities with high-resolution spatiotemporal dispersion and chemical transformation approaches. These methods provide a clearer picture of SOA formation dynamics in urban areas. While SOA cannot always be directly linked to specific sources, advances such as Aerosol Mass Spectrometry (AMS) have enabled partial source attribution based on composition profiles, distinguishing between biogenic, anthropogenic, or combustion-related contributions. Similarly, although SOAs are not individually regulated, their precursors and total (PM are typically targeted by air quality regulations. This study contributes to the effort of improving mechanistic understanding of SOA formation, particularly from key anthropogenic precursors like toluene, and can support the refinement of regulatory strategies by improving attribution and prediction of SOA impacts. Moreover, considering the potential variability in health impacts from different SOA types, identifying precursor-specific contributions is increasingly important for public health and environmental policy.

Code and data availability

The codes and datasets in this publication are available to the community, and they can be accessed by request to the corresponding author.

Disclosure statement

During the preparation of this work, the authors used ChatGPT 3.5 only to improve the readability and language of the manuscript. After using these tools, the authors reviewed and edited the content as needed and take full responsibility for the content of the publication.

Funding

The research was funded by the Helmholtz Association of German Research Centres, through the GRACE foundation under
Funding number 51, in the frameworks of HEPTA project.

CRediT authorship contribution statement

Giannis Ioannidis: Conceptualization, Data curation, Formal analysis, Investigation, Methodology, Software, Validation, Visualization, Writing – original draft, Writing – review & editing. **Nikoletta Bouloti:** Investigation, Methodology, Writing – original draft. **Paul Tremper:** Data curation. **Chaofan Li:** Data curation. **Christos Boikos:** Investigation, Software. **Nikolaos Rapkos:** Investigation, Software. **Till Riedel:** Conceptualization, Data curation. **Miikka Dal Maso:** Conceptualization, Methodology, Supervision, Writing – review & editing. **Leonidas Ntziachristos:** Conceptualization, Investigation, Methodology, Supervision, Writing – original draft, Writing – review & editing.

Declaration of competing interest

The authors declare the following financial interests/personal relationships which may be considered as potential competing interestsGiannis Ioannidis reports financial support was provided by Helmholtz Association of German Research Centres. If there are other authors, they declare that they have no known competing financial interests or personal relationships that could have appeared to influence the work reported in this paper.

Acknowledgements

This study was conducted as part of the HEPTA project in the context of “Air Quality in Smart Cities” and is supported by the GRACE organization. GRAZ university of technology provided traffic information and the KIT air quality data. GECKO-A model results obtained from J. Lee-Taylor and C. Drews, Atmospheric Chemistry Observations and Modelling (ACOM), NSF-NCAR, https://www.acom.ucar.edu/gecko/output-library.shtml, accessed 12/01/2022. By using the CFD software we acknowledge OPENFOAM® as a registered trademark of OpenCFD Limited, producer and distributor of the OpenFOAM software via www.openfoam.com. The authors used ChatGPT 3.5 only to improve the readability and language of this work.

Appendix A. Supplementary data

Supplementary data to this article can be found online at https://doi.

org/10.1016/j.apr.2026.103096.

References

Ahmad, W., Coeur, C., Cuisset, A., Coddeville, P., Tomas, A., 2017. Effects of scavengers of criegee intermediates and OH radicals on the formation of secondary organic aerosol in the ozonolysis of limonene. J. Aerosol Sci. 110, 70–83. https://doi.org/10.1016/j.jaerosci.2017.05.010.

Altshuller, A.P., 1989. Ambient air hydroxyl radical concentrations: measurements and model predictions. J. Air Pollut. Control Assoc. 39 (5), 704–708. https://doi.org/10.1080/08940630.1989.10466556.

Antoniou, A., Ioannidis, G., Ntziachristos, L., 2024. Realistic simulation of air pollution in an urban area to promote environmental policies. Environ. Modell. Software 172. https://doi.org/10.1016/j.envsoft.2023.105918.

Aumont, B., Szopa, S., Madronich, S., 2005. Modelling the evolution of organic carbon during its gas-phase tropospheric oxidation: development of an explicit model based on a self generating approach. Atmos. Chem. Phys. 5. www.atmos-chem-phys.org/acp/5/2497/SRef-ID:1680-7324/acp/2005-5-2497EuropeanGeosciencesUnion.

Baklanov, A., Zhang, Y., 2020. Advances in air quality modeling and forecasting. Global Transitions 2, 261–270. https://doi.org/10.1016/j.glt.2020.11.001. KeAi Communications Co.

Bell, D.M., Wu, C., Bertrand, A., Graham, E., Schoonbaert, J., Giannoukos, S., Baltensperger, U., Prevot, A.S.H., Riipinen, I., El Haddad, I., Mohr, C., 2022. Particle-phase processing of α-pinene NO3secondary organic aerosol in the dark. Atmos. Chem. Phys. 22 (19), 13167–13182. https://doi.org/10.5194/acp-22-13167-2022.

Blocken, B., 2015. Computational fluid dynamics for urban physics: importance, scales, possibilities, limitations and ten tips and tricks towards accurate and reliable simulations. Build. Environ. 91, 219–245. https://doi.org/10.1016/j.buildenv.2015.02.015.

Boikos, C., Ioannidis, G., Rapkos, N., Tsegas, G., Katsis, P., Ntziachristos, L., 2025. Estimating daily road traffic pollution in Hong Kong using CFD modelling: validation and application. Build. Environ. 267, 112168. https://doi.org/10.1016/j.buildenv.2024.112168.

Boikos, C., Rapkos, N., Ioannidis, G., Oppo, S., Armengaud, A., Siamidis, P., Tsegas, G., Ntziachristos, L., 2024a. Factors affecting pedestrian-level ship pollution in port areas: CFD in the service of policy-making. Build. Environ. 258. https://doi.org/10.1016/j.buildenv.2024.111594.

Boikos, C., Siamidis, P., Oppo, S., Armengaud, A., Tsegas, G., Mellqvist, J., Conde, V., Ntziachristos, L., 2024b. Validating CFD modelling of ship plume dispersion in an urban environment with pollutant concentration measurements. Atmos. Environ. 319. https://doi.org/10.1016/j.atmosenv.2023.120261.

Bonifacio, H.F., Maghirang, R.G., Glasgow, L.A., 2014. Numerical simulation of transport of particles emitted from ground-level area source using AERMOD and CFD. Eng. Appl. Comput. Fluid Mech. 8 (4), 488–502. https://doi.org/10.1080/19942060.2014.11083302.

Brégonzio-Rozier, L., Siekmann, F., Giorio, C., Pangui, E., Morales, S.B., Temime-Roussel, B., Gratien, A., Michoud, V., Ravier, S., Cazaunau, M., Tapparo, A., Monod, A., Doussin, J.F., 2015. Gaseous products and secondary organic aerosol formation during long term oxidation of isoprene and methacrolein. Atmos. Chem. Phys. 15 (6), 2953–2968. https://doi.org/10.5194/acp-15-2953-2015.

Brines, M., Dall'Osto, M., Amato, F., Minguillón, M.C., Karanasiou, A., Grimalt, J.O., Alastuey, A., Querol, X., van Drooge, B.L., 2019. Source apportionment of urban PM1 in Barcelona during SAPUSS using organic and inorganic components. Environ. Sci. Pollut. Control Ser. 26 (31), 32114–32127. https://doi.org/10.1007/s11356-019-06199-3.

Cain, K.P., Liangou, A., Davidson, M.L., Pandis, S.N., 2021. α-pinene, limonene, and cyclohexene secondary organic aerosol hygroscopicity and oxidation level as a function of volatility. Aerosol Air Qual. Res. 21 (5). https://doi.org/10.4209/aaqr.2020.08.0511.

Calvert, J.G., Atkinson, R., Becker, K.H., Kamens, R.M., Seinfeld, J.H., Wallington, T.J., Yarwood, G., 2002. The Mechanisms of Atmospheric Oxidation of Aromatic Hydrocarbons. Oxford University Press. https://doi.org/10.1093/oso/9780195146288.001.0001.

Camredon, M., Aumont, B., Lee-Taylor, J., Madronich, S., 2007. The SOA/VOC/NO x system: an explicit model of secondary organic aerosol formation. Atmos. Chem. Phys. 7. www.atmos-chem-phys.net/7/5599/2007/.

Carlton, A.G., Wiedinmyer, C., Kroll, J.H., 2009. Atmospheric chemistry and physics A review of secondary organic aerosol (SOA) formation from isoprene. Atmos. Chem. Phys. 9. www.atmos-chem-phys.net/9/4987/2009/.

Chan, A.W.H., Kautzman, K.E., Chhabra, P.S., Surratt, J.D., Chan, M.N., Crounse, J.D., Urten, A.K., Wennberg, P.O., Flagan, R.C., Seinfeld, J.H., 2009. Secondary organic aerosol formation from photooxidation of naphthalene and alkylnaphthalenes: implications for oxidation of intermediate volatility organic compounds (IVOCs). Atmos. Chem. Phys. 9. www.atmos-chem-phys.net/9/3049/2009/.

Chen, T., Zhang, P., Ma, Q., Chu, B., Liu, J., Ge, Y., He, H., 2022. Smog chamber study on the role of NO xin SOA and O3Formation from aromatic hydrocarbons. Environ. Sci. Technol. 56 (19), 13654–13663. https://doi.org/10.1021/acs.est.2c04022.

Cho, C., Fuchs, H., Hofzumahaus, A., Holland, F., Bloss, W.J., Bohn, B., Dorn, H.P., Glowania, M., Hohaus, T., Liu, L., Monks, P.S., Niether, D., Rohrer, F., Sommariva, R., Tan, Z., Tillmann, R., Kiendler-Scharr, A., Wahner, A., Novelli, A., 2023. Experimental chemical budgets of OH, HO2, and RO2 radicals in rural air in Western Germany during the JULIAC campaign 2019. Atmos. Chem. Phys. 23 (3), 2003–2033. https://doi.org/10.5194/acp-23-2003-2023.

Claeys, M., Maenhaut, W., 2021. Secondary organic aerosol formation from isoprene: selected research, historic account and state of the art. Atmosphere 12 (6). https://doi.org/10.3390/atmos12060728. MDPI AG.

Couvidat, F., Kim, Y., Sartelet, K., Seigneur, C., Marchand, N., Sciare, J., 2013. Modeling secondary organic aerosol in an urban area: application to Paris, France. Atmos. Chem. Phys. 13 (2), 983–996. https://doi.org/10.5194/acp-13-983-2013.

Dal Maso, M., Liao, L., Wildt, J., Kiendler-Scharr, A., Kleist, E., Tillmann, R., Sipilä, M., Hakala, J., Lehtipalo, K., Ehn, M., Kerminen, V.M., Kulmala, M., Worsnop, D., Mentel, T., 2016. A chamber study of the influence of boreal BVOC emissions and sulfuric acid on nanoparticle formation rates at ambient concentrations. Atmos. Chem. Phys. 16 (4), 1955–1970. https://doi.org/10.5194/acp-16-1955-2016.

Deng, W., Liu, T., Zhang, Y., Situ, S., Hu, Q., He, Q., Zhang, Z., Lü, S., Bi, X., Wang, X., Boreave, A., George, C., Ding, X., Wang, X., 2017. Secondary organic aerosol formation from photo-oxidation of toluene with NOx and SO2: chamber simulation with purified air versus urban ambient air as matrix. Atmos. Environ. 150, 67–76. https://doi.org/10.1016/j.atmosenv.2016.11.047.

Dommen, J., Metzger, A., Duplissy, J., Kalberer, M., Alfarra, M.R., Gascho, A., Weingartner, E., Prevot, A.S.H., Verheggen, B., Baltensperger, U., 2006. Laboratory observation of oligomers in the aerosol from isoprene/NO x photooxidation. Geophys. Res. Lett. 33 (13). https://doi.org/10.1029/2006GL026523.

Du, Y., Blocken, B., Abbasi, S., Pirker, S., 2021. Efficient and high-resolution simulation of pollutant dispersion in complex urban environments by island-based recurrence CFD. Environ. Modell. Software 145. https://doi.org/10.1016/j.envsoft.2021.105172.

Ehn, M., Thornton, J.A., Kleist, E., Sipilä, M., Junninen, H., Pullinen, I., Springer, M., Rubach, F., Tillmann, R., Lee, B., Lopez-Hilfiker, F., Andres, S., Acir, I.H., Rissanen, M., Jokinen, T., Schobesberger, S., Kangasluoma, J., Kontkanen, J., Nieminen, T., et al., 2014. A large source of low-volatility secondary organic aerosol. Nature 506 (7489), 476–479. https://doi.org/10.1038/nature13032.

Eluri, S., Cappa, C.D., Friedman, B., Farmer, D.K., Jathar, S.H., 2018. Modeling the formation and composition of secondary organic aerosol from diesel exhaust using parameterized and semi-explicit chemistry and thermodynamic models. Atmos. Chem. Phys. 18 (19), 13813–13838. https://doi.org/10.5194/acp-18-13813-2018.

Gkirmpas, P., Tsegas, G., Ioannidis, G., Vlachokostas, C., Moussiopoulos, N., 2024. Identification of an unknown stationary emission source in urban geometry using bayesian inference. Atmosphere 15 (8), 871. https://doi.org/10.3390/atmos15080871.

Hallquist, M., Wenger, J.C., Baltensperger, U., Rudich, Y., Simpson, D., Claeys, M., Dommen, J., Donahue, N.M., George, C., Goldstein, A.H., Hamilton, J.F., Herrmann, H., Hoffmann, T., Iinuma, Y., Jang, M., Jenkin, M.E., Jimenez, J.L., Kiendler-Scharr, A., Maenhaut, W., et al., 2009. The formation, properties and impact of secondary organic aerosol: current and emerging issues. Atmos. Chem. Phys. 9. www.atmos-chem-phys.net/9/5155/2009/.

Han, L., Siekmann, F., Zetzsch, C., 2018. Rate constants for the reaction of OH radicals with hydrocarbons in a smog chamber at low atmospheric temperatures. Atmosphere 9 (8). https://doi.org/10.3390/atmos9080320.

Hodzic, A., Jimenez, J.L., Madronich, S., Aiken, A.C., Bessagnet, B., Curci, G., Fast, J., Lamarque, J.-F., Onasch, T.B., Roux, G., Schauer, J.J., Stone, E.A., Ulbrich, I.M., 2009. Modeling organic aerosols during MILAGRO: importance of biogenic secondary organic aerosols. Atmos. Chem. Phys. 9. www.atmos-chem-phys.net/9/6949/2009/.

Hu, Y., Xu, F., Gao, Z., 2022. A comparative study of the simulation accuracy and efficiency for the urban wind environment based on CFD plug-ins integrated into architectural design platforms. Buildings 12 (9). https://doi.org/10.3390/buildings12091487.

Huang, H., Hu, H., Zhang, J., Liu, X., 2020. Characteristics of volatile organic compounds from vehicle emissions through on–road test in Wuhan, China. Environ. Res. 188. https://doi.org/10.1016/j.envres.2020.109802.

Ioannidis, G., Li, C., Tremper, P., Riedel, T., Ntziachristos, L., 2024a. Application of CFD modelling for pollutant dispersion at an urban traffic hotspot. Atmosphere 15 (1). https://doi.org/10.3390/atmos15010113.

Ioannidis, G., Tremper, P., Li, C., Riedel, T., Rapkos, N., Boikos, C., Ntziachristos, L., 2024b. Integrating cost-effective measurements and CFD modeling for accurate air quality assessment. Atmosphere 15 (9), 1056. https://doi.org/10.3390/atmos15091056.

Ioannidis, G., Tremper, P., Li, C., Riedel, T., Rapkos, N., Boikos, C., Ntziachristos, L., 2025. Evaluating the spatial coverage of air quality monitoring stations using computational fluid dynamics. Atmosphere 16 (3). https://doi.org/10.3390/atmos16030326.

Jeanjean, A., Buccolieri, R., Eddy, J., Monks, P., Leigh, R., 2017. Air quality affected by trees in real street canyons: the case of marylebone neighbourhood in central London. Urban For. Urban Green. 22, 41–53. https://doi.org/10.1016/j.ufug.2017.01.009.

Jia, L., Xu, Y.F., 2018. Different roles of water in secondary organic aerosol formation from toluene and isoprene. Atmos. Chem. Phys. 18 (11), 8137–8154. https://doi.org/10.5194/acp-18-8137-2018.

Jiang, F., Liu, Q., Huang, X., Wang, T., Zhuang, B., Xie, M., 2012. Regional modeling of secondary organic aerosol over China using WRF/Chem. J. Aerosol Sci. 43 (1), 57–73. https://doi.org/10.1016/j.jaerosci.2011.09.003.

Ju, K., Lu, L., Wang, W., Chen, T., Yang, C., Zhang, E., Xu, Z., Li, S., Song, J., Pan, J., Guo, Y., 2022. Causal effects of air pollution on mental health among Adults——An exploration of susceptible populations and role of physical activity based on a longitudinal nationwide cohort in China. Environ. Res., 114761 https://doi.org/10.1016/j.envres.2022.114761.

Kadaverugu, R., Sharma, A., Matli, C., Biniwale, R., 2019. High resolution urban air quality modeling by coupling CFD and mesoscale models: a review. Asia-Pacific

Journal of Atmospheric Sciences 55 (4), 539–556. https://doi.org/10.1007/s13143-019-00110-3. Korean Meteorological Society.
Kang, E., Root, M.J., Toohey, D.W., Brune, W.H., 2007. Atmospheric chemistry and physics introducing the concept of potential Aerosol mass (PAM). Atmos. Chem. Phys. 7. www.atmos-chem-phys.net/7/5727/2007/.
Kim, H., Barkey, B., Paulson, S.E., 2012. Real refractive indices and formation yields of secondary organic aerosol generated from photooxidation of limonene and α-pinene: the effect of the HC/NO x ratio. J. Phys. Chem. A 116 (24), 6059–6067. https://doi.org/10.1021/jp301302z.
Lambe, A.T., Ahern, A.T., Williams, L.R., Slowik, J.G., Wong, J.P.S., Abbatt, J.P.D., Brune, W.H., Ng, N.L., Wright, J.P., Croasdale, D.R., Worsnop, D.R., Davidovits, P., Onasch, T.B., 2011. Characterization of aerosol photooxidation flow reactors: heterogeneous oxidation, secondary organic aerosol formation and cloud condensation nuclei activity measurements. Atmos. Meas. Tech. 4 (3), 445–461. https://doi.org/10.5194/amt-4-445-2011.
Lamkaddam, H., Gratien, A., Pangui, E., Cazaunau, M., Picquet-Varrault, B., Doussin, J. F., 2017. High-NOx photooxidation of n-Dodecane: temperature dependence of SOA formation. Environ. Sci. Technol. 51 (1), 192–201. https://doi.org/10.1021/acs.est.6b03821.
Lannuque, V., Camredon, M., Couvidat, F., Hodzic, A., Valorso, R., Madronich, S., Bessagnet, B., Aumont, B., 2018. Exploration of the influence of environmental conditions on secondary organic aerosol formation and organic species properties using explicit simulations: development of the VBS-GECKO parameterization. Atmos. Chem. Phys. 18 (18), 13411–13428. https://doi.org/10.5194/acp-18-13411-2018.
Lelieveld, J., Evans, J.S., Fnais, M., Giannadaki, D., Pozzer, A., 2015. The contribution of outdoor air pollution sources to premature mortality on a global scale. Nature 525 (7569), 367–371. https://doi.org/10.1038/nature15371.
Li, J., Carlson, B.E., Yung, Y.L., Lv, D., Hansen, J., Penner, J.E., Liao, H., Ramaswamy, V., Kahn, R.A., Zhang, P., Dubovik, O., Ding, A., Lacis, A.A., Zhang, L., Dong, Y., 2022. Scattering and absorbing aerosols in the climate system. Nat. Rev. Earth Environ. 3 (6), 363–379. https://doi.org/10.1038/s43017-022-00296-7. Springer Nature.
Li, J., Li, H., Li, K., Chen, Y., Zhang, H., Zhang, X., Wu, Z., Liu, Y., Wang, X., Wang, W., Ge, M., 2021. Enhanced secondary organic aerosol formation from the photo-oxidation of mixed anthropogenic volatile organic compounds. Atmos. Chem. Phys. 21 (10), 7773–7789. https://doi.org/10.5194/acp-21-7773-2021.
Li, J., Li, Y., Wang, Z., Zhu, J., Kong, L., Li, J., Wu, H., Li, L., Tang, X., Cheng, Z., Zhang, L., Gan, P., Pan, X., Yang, W., Cao, K., Zheng, J., 2025. Next generation air quality models: dynamical mesh, new insights into mechanism, datasets and applications. Curr. Pollut. Rep. 11 (1). https://doi.org/10.1007/s40726-025-00355-9. Springer Science and Business Media Deutschland GmbH.
Loza, C.L., Craven, J.S., Yee, L.D., Coggon, M.M., Schwantes, R.H., Shiraiwa, M., Zhang, X., Schilling, K.A., Ng, N.L., Canagaratna, M.R., Ziemann, P.J., Flagan, R.C., Seinfeld, J.H., 2014. Secondary organic aerosol yields of 12-carbon alkanes. Atmos. Chem. Phys. 14 (3), 1423–1439. https://doi.org/10.5194/acp-14-1423-2014.
Mehta, D., Hazarika, N., Srivastava, A., 2020. Diurnal variation of BTEX at road traffic intersection points in Delhi, India: source, ozone formation potential, and health risk assessment. Environ. Sci. Pollut. Control Ser. 27 (10), 11093–11104. https://doi.org/10.1007/s11356-019-07495-8.
Miao, Y., Liu, S., Zheng, Y., Wang, S., Li, Y., 2014. Numerical study of traffic pollutant dispersion within different street canyon configurations. Adv. Meteorol. 2014. https://doi.org/10.1155/2014/458671.
Ng, N.L., Chhabra, P.S., Chan, A.W.H., Surratt, J.D., Kroll, J.H., Kwan, A.J., Mccabe, D. C., Wennberg, P.O., Sorooshian, A., Murphy, S.M., Dalleska, N.F., Flagan, R.C., Seinfeld, J.H., 2007a. Atmospheric chemistry and physics effect of NO x level on secondary organic aerosol (SOA) formation from the photooxidation of terpenes. Atmos. Chem. Phys. 7. www.atmos-chem-phys.net/7/5159/2007/.
Ng, N.L., Kroll, J.H., Chan, A.W.H., Chhabra, P.S., Flagan, R.C., Seinfeld, J.H., 2007b. Secondary organic aerosol formation from m-xylene, toluene, and benzene. Atmos. Chem. Phys. 7. www.atmos-chem-phys.net/7/3909/2007/.
Nguyen, T.B., Roach, P.J., Laskin, J., Laskin, A., Nizkorodov, S.A., 2011. Effect of humidity on the composition of isoprene photooxidation secondary organic aerosol. Atmos. Chem. Phys. 11 (14), 6931–6944. https://doi.org/10.5194/acp-11-6931-2011.
Oliva, G., Pahunang, R.R., Vigliotta, G., Zarra, T., Ballesteros, F.C., Mariniello, A., Buonerba, A., Belgiorno, V., Naddeo, V., 2023. Advanced treatment of toluene emissions with a cutting-edge algal bacterial photo-bioreactor: performance assessment in a circular economy perspective. Sci. Total Environ. 878. https://doi.org/10.1016/j.scitotenv.2023.163005.
Pantusheva, M., Mitkov, R., Hristov, P.O., Petrova-Antonova, D., 2022. Air pollution dispersion modelling in urban environment using CFD: a systematic review. Atmosphere 13 (10). https://doi.org/10.3390/atmos13101640.
Peralta, C., Nugusse, H., Kokilavani, S.P., Schmidt, J., Stoevesandt, B., 2014. Validation of the simpleFoam (RANS) solver for the atmospheric boundary layer in complex terrain. ITM Web of Conferences 2, 01002. https://doi.org/10.1051/itmconf/20140201002.
Pope, C.A., Dockery, D.W., 2006. Health effects of fine particulate air pollution: lines that connect. J. Air Waste Manag. Assoc. 56 (6), 709–742. https://doi.org/10.1080/10473289.2006.10464485.
Poupkou, A., Kontos, S., Liora, N., Tsiaousidis, D., Kapsomenakis, I., Solomos, S., Liakakou, E., Athanasopoulou, E., Grivas, G., Bougiatioti, A., Petrinoli, K., Diapouli, E., Vasilatou, V., Papagiannis, S., Progiou, A., Kalabokas, P., Melas, D., Mihalopoulos, N., Gerasopoulos, E., et al., 2025. Investigating the role of organic aerosol schemes in the simulation of atmospheric particulate matter in a large mediterranean urban agglomeration. Sustainability 17 (6). https://doi.org/10.3390/su17062619.
Pullinen, I., Schmitt, S., Kang, S., Sarrafzadeh, M., Schlag, P., Andres, S., Kleist, E., Mentel, T.F., Rohrer, F., Springer, M., Tillmann, R., Wildt, J., Wu, C., Zhao, D., Wahner, A., Kiendler-Scharr, A., 2020. Impact of NOxon secondary organic aerosol (SOA) formation from α-pinene and β-pinene photooxidation: the role of highly oxygenated organic nitrates. Atmos. Chem. Phys. 20 (17), 10125–10147. https://doi.org/10.5194/acp-20-10125-2020.
Pye, H.O.T., Murphy, B.N., Xu, L., Ng, N.L., Carlton, A.G., Guo, H., Weber, R., Vasilakos, P., Wyat Appel, K., Hapsari Budisulistiorini, S., Surratt, J.D., Nenes, A., Hu, W., Jimenez, J.L., Isaacman-Vanwertz, G., Misztal, P.K., Goldstein, A.H., 2017. On the implications of aerosol liquid water and phase separation for organic aerosol mass. Atmos. Chem. Phys. 17 (1), 343–369. https://doi.org/10.5194/acp-17-343-2017.
Rapkos, N., Boikos, C., Ioannidis, G., Ntziachristos, L., 2024. Direct deposition of air pollutants in the wake of container vessels: the missing term in the environmental impact of shipping. Atmos. Pollut. Res. 15 (3), 102013. https://doi.org/10.1016/j.apr.2023.102013.
Rapkos, N., Weigelt, A., Beecken, J., Ntziachristos, L., 2023. Method to identify fuel sulphur content (FSC) violations of ongoing vessels using CFD modelling. Atmos. Environ. 309. https://doi.org/10.1016/j.atmosenv.2023.119912.
Rivas, E., Santiago, J.L., Lechón, Y., Martín, F., Ariño, A., Pons, J.J., Santamaría, J.M., 2019. CFD modelling of air quality in pamplona city (Spain): assessment, stations spatial representativeness and health impacts valuation. Sci. Total Environ. 649, 1362–1380. https://doi.org/10.1016/j.scitotenv.2018.08.315.
Sarrafzadeh, M., Wildt, J., Pullinen, I., Springer, M., Kleist, E., Tillmann, R., Schmitt, S. H., Wu, C., Mentel, T.F., Zhao, D., Hastie, D.R., Kiendler-Scharr, A., 2016. Impact of NOx and OH on secondary organic aerosol formation from β-pinene photooxidation. Atmos. Chem. Phys. 16 (17), 11237–11248. https://doi.org/10.5194/acp-16-11237-2016.
Sasidharan, S., He, Y., Akherati, A., Li, Q., Li, W., Cocker, D., McDonald, B.C., Coggon, M. M., Seltzer, K.M., Pye, H.O.T., Pierce, J.R., Jathar, S.H., 2023. Secondary organic aerosol formation from volatile chemical product emissions: model parameters and contributions to anthropogenic aerosol. Environ. Sci. Technol. 57 (32), 11891–11902. https://doi.org/10.1021/acs.est.3c00683.
Singh, S., Li, Z., 2007. Kinetics investigation of OH reaction with isoprene at 240-340 K and 1-3 torr using the relative rate/discharge flow/mass spectrometry technique. J. Phys. Chem. A 111 (46), 11843–11851. https://doi.org/10.1021/jp074148h.
Song, M., Zhang, C., Wu, H., Mu, Y., Ma, Z., Zhang, Y., Liu, J., Li, X., 2019. The influence of OH concentration on SOA formation from isoprene photooxidation. Sci. Total Environ. 650, 951–957. https://doi.org/10.1016/j.scitotenv.2018.09.084.
Srivastava, D., Vu, T.V., Tong, S., Shi, Z., Harrison, R.M., 2022. Formation of secondary organic aerosols from anthropogenic precursors in laboratory studies. npj Clim. Atmos. Sci. 5 (1). https://doi.org/10.1038/s41612-022-00238-6. Nature Research.
Surratt, J.D., Murphy, S.M., Kroll, J.H., Ng, N.L., Hildebrandt, L., Sorooshian, A., Szmigielski, R., Vermeylen, R., Maenhaut, W., Claeys, M., Flagan, R.C., Seinfeld, J. H., 2006. Chemical composition of secondary organic aerosol formed from the photooxidation of isoprene. J. Phys. Chem. A 110 (31), 9665–9690. https://doi.org/10.1021/jp061734m.
Tchepel, O., Costa, A.M., Martins, H., Ferreira, J., Monteiro, A., Miranda, A.I., Borrego, C., 2010. Determination of background concentrations for air quality models using spectral analysis and filtering of monitoring data. Atmos. Environ. 44 (1), 106–114. https://doi.org/10.1016/j.atmosenv.2009.08.038.
Tominaga, Y., Stathopoulos, T., 2007. Turbulent schmidt numbers for CFD analysis with various types of flowfield. Atmos. Environ. 41 (37), 8091–8099. https://doi.org/10.1016/j.atmosenv.2007.06.054.
Trindade da Silva, F., Costa Reis, N., Santos, J.M., Valentim Goulart, E., Simões Maciel, F., Bragança, L., Engel de Alvarez, C., 2021. Atmospheric dispersion and urban planning: an interdisciplinary approach to city modeling. Sustain. Cities Soc. 70. https://doi.org/10.1016/j.scs.2021.102882.
Wu, L., Wu, B., Ling, Z., Shao, M., Wang, X., 2025. Development of SOA modules in the WRF-Chem model and evaluation of the key formation pathways of SOA and associated health risk over mainland China. Environ. Int. 202. https://doi.org/10.1016/j.envint.2025.109662.
Yang, Y., Gu, M., Chen, S., Jin, X., 2009. New inflow boundary conditions for modelling the neutral equilibrium atmospheric boundary layer in computational wind engineering. J. Wind Eng. Ind. Aerod. 97 (2), 88–95. https://doi.org/10.1016/j.jweia.2008.12.001.
Zhang, X., Schwantes, R.H., McVay, R.C., Lignell, H., Coggon, M.M., Flagan, R.C., Seinfeld, J.H., 2015. Vapor wall deposition in Teflon chambers. Atmos. Chem. Phys. 15 (8), 4197–4214. https://doi.org/10.5194/acp-15-4197-2015.
Zhou, C., Jang, M., Yu, Z., 2019. Simulation of SOA formation from the photooxidation of monoalkylbenzenes in the presence of aqueous aerosols containing electrolytes under various NOx levels. Atmos. Chem. Phys. 19 (8), 5719–5735. https://doi.org/10.5194/acp-19-5719-2019.
Zou, Z., Chen, Q., Xia, M., Yuan, Q., Chen, Y., Wang, Y., Xiong, E., Wang, Z., Wang, T., 2023. OH measurements in the coastal atmosphere of South China: possible missing OH sinks in aged air masses. Atmos. Chem. Phys. 23 (12), 7057–7074. https://doi.org/10.5194/acp-23-7057-2023.